Remote Sensing of Environment 201 (2017) 133–147

Contents lists available at ScienceDirect

Remote Sensing of Environment

journal homepage: www.elsevier.com/locate/rse

Oil spill detection by imaging radars: Challenges and pitfalls

Werner Alpers[a,*], Benjamin Holt[b], Kan Zeng[c]

[a] Institute of Oceanography, University of Hamburg, Bundesstrasse 53, 20146 Hamburg, Germany
[b] Jet Propulsion Laboratory, California Institute of Technology, 4800 Oak Grove Drive, Pasadena, CAL 91109, USA
[c] Ocean Remote Sensing Institute, Ocean University of China, 5 Yushan Road, Qingdao 266003, China

ARTICLE INFO

Keywords:
Oil spills
Biogenic slicks
SAR
Polarimetry
Co-polarized phase difference

ABSTRACT

Criteria for discriminating between radar signatures of oil films and biogenic slicks visible on synthetic aperture radar (SAR) images of the sea surface as dark patches are critically reviewed. We question the often claimed high success rate of oil spill detection algorithms using single-polarization SARs because the SAR images used to train these algorithms are based usually on subjective interpretation and are not validated by on-site inspections or multi-sensor measurements carried out from oil pollution surveillance planes. Furthermore, we doubt that polarimetric parameters derived from fully-polarimetric SAR data, like entropy, anisotropy, and mean scattering angle, are beneficial for discriminating between mineral oil films and biogenic slicks. We challenge the often-made claim that another scattering mechanism than Bragg scattering applies for radar backscattering from mineral oil films than from biogenic slicks. This view is supported by data acquired by the Unmanned Aerial Vehicle Synthetic Aperture Radar (UAVSAR) of NASA/JPL, which operates at L-band and has an extremely low noise floor. We suspect that opposing results obtained from previous analyses of spaceborne polarimetric SAR data are caused by the high noise floors of the spaceborne SARs. However, most of the analyzed spaceborne polarimetric data were not acquired at L-band, but at C-and X-band. On the other hand, differences in the statistical behavior of the radar backscattering could be real due to the fact that, other than biogenic surface films, mineral oil films, can form multi-layers, whose thickness can vary within an oil patch. Radar backscattering from emulsion layers can also fluctuate due to variations of the oil/water mixture ratio. These effects could cause an increase of the standard deviation (STD) of the co-polarized phase difference (CPD) for scattering at mineral oil films and emulsions. In the special case of thick oil layers or oil/water emulsion layers, where the radar is sensitive to the dielectric constant of the oil, discrimination becomes possible due the fact that Bragg scattering depends on the dielectric constant of the scattering medium.

1. Introduction

Pollution of the sea surface by mineral or petroleum oil is a major environmental concern, as dramatically shown by the Deepwater Horizon (DWH) platform oil spill accident in 2010 in the Gulf of Mexico (Leifer et al., 2012; Garcia-Pineda et al., 2013). Despite the International Convention for the Prevention of Pollution from Ships (MARPOL 73/78), which entered into force in 1983, large quantities of mineral oil are still being discharged illegally from ships into the sea. Most of the anthropogenic oil pollution encountered at sea does not originate from ship accidents, but from routine ship operations, like tank washing, and engine effluent discharges (sludge). But there are also other anthropogenic sources of oil pollution: from offshore oil platforms, oil terminals, industrial plants, pipelines, and refineries. From the environmental point of view, there is a pressing need to monitor illegal discharges of mineral oil in order to reduce oil pollution at sea. It is estimated that at least 3000 major illegal mineral oil dumping incidents take place in the European waters per year, amounting to a total amounts of between 15,000 and 60,000 tons in the North Sea (Carpenter, 2016). To this end, spaceborne and airborne remote sensing techniques are being applied. Imaging radars, like the real aperture radar (RAR) and the synthetic aperture radar (SAR), are key instruments for oil spill monitoring, because they yield data independent of the time of the day and independent of weather conditions (see, e.g., Alpers and Espedal, 2004). However, identifying unambiguously mineral oil films on radar images is a very demanding task. A plethora of papers have been published in the last 30 years with the aim to establish algorithms to extract information on oil pollution from radar images.

Mineral oil spills floating on the sea surface are detectable by imaging radars because they damp the short surface waves that are responsible for the radar backscattering. Oil spills appear as dark areas

* Corresponding author.
E-mail addresses: werner.alpers@uni-hamburg.de (W. Alpers), benjamin.m.holt@jpl.nasa.gov (B. Holt), zengkan@ouc.edu.cn (K. Zeng).

http://dx.doi.org/10.1016/j.rse.2017.09.002
Received 10 October 2016; Received in revised form 22 August 2017; Accepted 2 September 2017
0034-4257/ © 2017 The Authors. Published by Elsevier Inc. This is an open access article under the CC BY-NC-ND license (http://creativecommons.org/licenses/BY-NC-ND/4.0/).

on radar images. The gray level in SAR images is related to the normalized radar cross section (NRCS or σ^o) representing the power of the backscattered radar signal. However, dark areas or areas of reduced NRCS values, do not always originate from mineral oil spills. They can, e.g., originate from: 1) natural surface films which are produced by plankton or fish, 2) low winds as often encountered in the lee of islands or coastal mountains, 3) cold upwelling water which changes the stability of the air-sea interface, 4) divergent flow regimes associated, e.g., with internal waves, tidal flow over underwater sand banks, and oceanic eddies, 5) dry-fallen sand banks during ebb tide, 6) turbulent water as encountered in ship wakes, 7) rain drops impinging onto the sea surface generating turbulence in the upper water layer, which damp the short waves, 8) grease or frazil sea ice, 9) discharged waste water from land-based industrial or urban plants (sewage plants), 10) storm water (flowing from land into the sea after strong rain events carrying surface active material, 11) floating macro-algae including sargassum and kelp, 12) plant oil spilled into the sea during tank cleaning of ships transporting palm oil, or 13) fish oil as encountered during fishing operations. The radar signatures caused by these phenomena are called "oil spill look-alikes". Pollution due to plant oil, in particular from palm oil, is usually not considered (or forgotten) in studies of oil pollution using radars. They also give rise to dark patches on radar images similarly to mineral oil. There exists a large fleet of tankers transporting palm oil. (Palm oil is used in Europe mainly (45%) to make diesel oil and the quantity shipped to Europe has increased from 456,000 tons in 2010 to 3.2 million tons in 2014). The tankers clean their tanks usually after leaving their port of destination, which is at present not illegal. Therefore it is expected that often dark patches visible on radar images taken close to ports do not originate from mineral oil, but from palm oil.

The great challenge is to single out those dark areas visible on SAR images of the sea surface that originate from oil pollution and not from oil spill look-alikes (Brekke and Solberg, 2005). The most challenging task is to separate radar signatures caused by mineral oil spills from those caused by biogenic surface films. Many remote sensing scientists have accepted this challenge and have developed discrimination algorithms based on differing criteria (see, e.g., Brekke and Solberg, 2008). First they used radar images that were acquired at a single polarization and developed discrimination algorithms based on 1) the degree of the NRCS reduction relative to the background, 2) the position/shape of the dark area, and 3) the texture of the dark feature. But it turned out that algorithms based on these properties often gave unsatisfactory results (false alarms). The main deficiency of these algorithms is that they often fail to discriminate between mineral oil spills and biogenic surface films.

After using single-polarization SARs for oil spill detection, which is the preferred approach in terms of sensor and operational costs, with moderate success, remote sensing scientists had hoped to achieve better success rates by using multi-frequency or/and multi-polarization SARs. A multi-frequency/multi-polarimetric SAR was first flown in space during the SIR-C/X-SAR Space Shuttle missions in 1994. During this mission, experiments were carried out with the aim to explore whether multi-frequency SARs were capable of discriminating between mineral oil films and monomolecular surface films (for details see Gade et al., 1998b). The rationale behind this approach was that the reduction of the NRCS caused by monomolecular surface films have another dependence on Bragg wavenumber than mineral oil films due to Marangoni damping (Alpers and Hühnerfuss, 1989; Gade et al., 1998a). It was concluded from this experiment that discrimination could be possible at low to moderate wind speeds, but not at high wind speeds (Gade et al., 1998b). The SIR-C/X-SAR data were also used to carry out polarimetric studies, but no positive results concerning discrimination between both types of surface films using polarimetry were obtained.

Since then, studies of oil film detection using multi-frequency SARs have not been pursued further, since after 1994 no multi-frequency SARs have been flown in space. But satellites carrying single-frequency polarimetric SARs, i.e., SARs that have the capability to emit and receive radar signals at different polarizations, are presently flying in space: on the German TerraSAR-X satellite, the Italian Cosmo-SkyMed satellites, the Canadian Radarsat-2 satellite, the Japanese ALOS-2 satellite, and the European Sentinel-1 satellites, and more multi-polarization SARs to be launched in the near future. The polarimetric SARs flown on TerraSAR-X, Radarsat-2, and ALOS-2 have the capability to operate in the fully-polarimetric (full-pol or full-quad) mode. In this mode, two orthogonal polarized radar signals (horizontal and vertical polarizations) are transmitted and are received at both polarizations. Thus it is possible to measure in this mode the full scattering matrix or Mueller matrix (see, e. g., Ulaby et al., 1992). However, when using multi-polarization SARs for oil spill detection, one has to keep in mind that their swath width is quite narrow, which is unfavorable for operational oil pollution monitoring, which aims at large coverage. Furthermore, using multiple SAR channels increase system and operational costs significantly.

In the last years, expectations have been high that fully-polarimetric SARs would turn out to be the ideal means to discriminate between mineral oil films and biogenic slicks. The rationale behind this approach is that the scattering mechanism for radar backscattering from sea surfaces covered with mineral oil films is different from that covered with biogenic slicks or from clean sea surfaces. It is claimed that in the case of scattering from mineral oil films Bragg scattering does not apply and that polarimetric SARs can detect this difference from Bragg scattering. To this end, various parameters (or features) calculated from polarimetric SAR data, like entropy (H), anisotropy (A), mean scattering angle (α), and copolarized phase difference (CPD) have been applied to reveal this difference.

Many papers have appeared in the last years dealing with oil spill detection using polarimetric SAR (for a review, the reader is referred to the paper of Migliaccio et al., 2015). However, the power of the backscattered radar signal from film covered sea surfaces is often so low, that it is near or even below the noise level of the instrument. As a consequence, the fully-polarimetric parameters calculated from these data could have been contaminated by instrument noise and therefore their usefulness for discrimination purposes is questionable, in particular when cross-polarization data are involved. In early papers, problems associated with the low signal-to-noise ratio of spaceborne polarimetric SARs have often been underestimated. However, measurements carried out over the Gulf of Mexico with the airborne Jet Propulsion Laboratory's (JPL) Uninhabited Aerial Vehicle Synthetic Aperture Radar (UAVSAR), which has an extremely low noise floor with a noise-equivalent sigma zero (NESZ) of -53 dB, have not confirmed previous results inferred from the analyses of the spaceborne polarimetric SAR data. In particular, they have not confirmed that for scattering from mineral oil films another scattering mechanism applies than for scattering at clean sea surfaces or sea surfaces covered with biogenic slicks (Minchew et al., 2012). However, there seem to be differences in the statistical behavior of the radar backscattering from mineral oil films and biogenic slicks as shown by Migliaccio et al. (2009), who analyzed data from the SARs flown on Space Shuttle during the SIR-C/X-SAR mission (Gade et al., 1998b), and by Skrunes et al. (2014) who analyzed Radarsat-2 SAR data. Assuming that these measured differences are real and not noise-related, we shall present in Section 5 a possible physical explanation for this experimental finding. We will attribute the difference in the statistical behavior of radar backscattering from mineral oil films and biogenic to the fact that mineral oil can form multi-layers and water/oil emulsions, while biogenic surface films can stay on the sea surface only as monolayers.

The paper is organized as follows: In Sections 2 and 3 we describe the physico-chemical differences between mineral oil films/emulsions and monomolecular biogenic slicks. In Section 4 we critically review conventional methods which are widely used for discriminating between mineral oil films and biogenic slicks. Then we review in Section 5 methods using statistical properties of the radar backscatter, in Section 6 methods using differences in the dielectric constant, and in Section 7

methods using polarimetric parameters for discrimination purposes. In Section 8 we report about experiences made in Europe and Canada with validations of oil spills detected on radar images, in Section 9 we discuss and summarize our results, and in Section 10 we present concluding remarks and give recommendations to improve oil spill detection algorithms.

2. Mineral oil spills and emulsions

Mineral oil films consist of a mixture of large number of chemical substances, including alkanes ("paraffins"), cycloalkanes, and aromatic compounds. The thickness of the oil layer can vary considerably within oil patches from < 1 μm to > 1 mm. After spilling or discharge, the oil film is continuous (connected), but then often breaks up quickly into fragments due to the action of waves, currents and turbulence (ITOPF, 2014), in particular at high wind speeds. Crude oil can rapidly form water-in-oil emulsions in which the water content is typically 50 to 75%. This is observed particularly often when the wind speed is > 7 m/s. The oil films usually drift away from their point of origin due to the action of currents, winds, and waves. The drifting and spreading of the oil film can be modeled as the superposition of advective and diffusive processes, where the advection is a linear combination of the surface current, the near-surface wind vector, and wave-induced Stokes drift. It has been found empirically that oil moves downwind of a few percent (typically 3.5%) of the wind velocity and at 100% of the current velocity (ASCE, 1996). Mineral oil films may drift on the sea surface for many days, weeks or even months during which their chemical composition changes due to weathering. Weathering is caused by evaporation, oxidation, emulsification, bio-degradation, dispersion, dissolution, and sedimentation, see Fig. 1. Most of the constituents of mineral oil have a hydrophobic character, i.e., the hydrophilic head group in the molecules is missing. As a consequence, mineral oil can persist on the ocean surface in the form of multi-layers. In contrast to biogenic slicks, which are monomolecular surface films, the surface waves do not generate surface tension gradients and thus Marangoni damping (see next section) is not active. The smooth sea surface in the presence of mineral oil films is caused by viscous damping of short gravity/capillary waves by the mineral oil film or the oil/water mixture, which has much higher viscosity than water. While the kinematic viscosity of water is around 1 cSt (cST = CentiStokes = $10^{-6}\,m^2\,s^{-1}$), the viscosity of mineral oil is much higher and varies strongly depending on the type of the mineral oil. For example, the kinematic viscosity of various types of mineral oil can range from diesel oil at 2.0–3.5 cSt, to Kuwait Light Crude Oil at 13.8 cSt, to heavy oils including North Slope Crude Oil at 58.4 cSt, and to bunker oil at > 500 cSt.

Due to the fact that mineral oil can form multilayers on the sea surface with variable thickness, can break up into fragments or form emulsion layers, the radar backscattering from mineral oil films exhibits more variations than radar backscattering from biogenic slicks. Due to the variable thickness and chemical composition of mineral oil films, the kinematic viscosity varies also within a mineral oil film. Since the kinematic viscosity determines the damping of the ocean waves, wave damping is also variable. The shorter the wavelength of the ocean waves, the stronger is the viscous damping. This implies that short ocean waves which are responsible for the radar backscattering (the Bragg waves which have wavelengths in the centimeter to decimeter range), exhibit strong variation in wave damping. An example of a mineral oil film showing variations in thickness is depicted in Fig. 2. In this case, the thickness of the film is of the order of the wavelength of visible light (0.4–0.7 μm). The (rainbow) color, called "oil sheen", is related to the thickness of the oil film and is caused by interference of light reflected at the lower and upper boundary of the oil film. Observers looking for oil pollution at sea from ships or airplanes often use the color of surface films to estimate their thickness (NOAA Hazmat, 2012). The damping of short gravity-capillary waves by thin oil layers floating on water was investigated theoretically by Jenkins and Jacobs (1997) and Jenkins and Dyste (1997). They showed that an oil film with a thickness d < 0.1 mm produces damping of the short-scale surface waves that is only slightly different from that of monomolecular surface films. However, for an oil film with a thickness between 0.1 mm and 1 mm, the bulk kinematic viscosity of the oil affects the damping, which increases linearly with film thickness. Thus, not only variations in the kinematic viscosity of the oil layer cause variations in the damping of

Fig. 2. Photo of a thin mineral oil film showing iridescent (rainbow) and silver sheens indicating different thickness of the oil film. (For interpretation of the references to color in this figure legend, the reader is referred to the web version of this article.)
Source: http://www.itopf.com/fileadmin/data/Documents/TIPS%20TAPS/TIP2FateofMarineOilSpills.pdf.

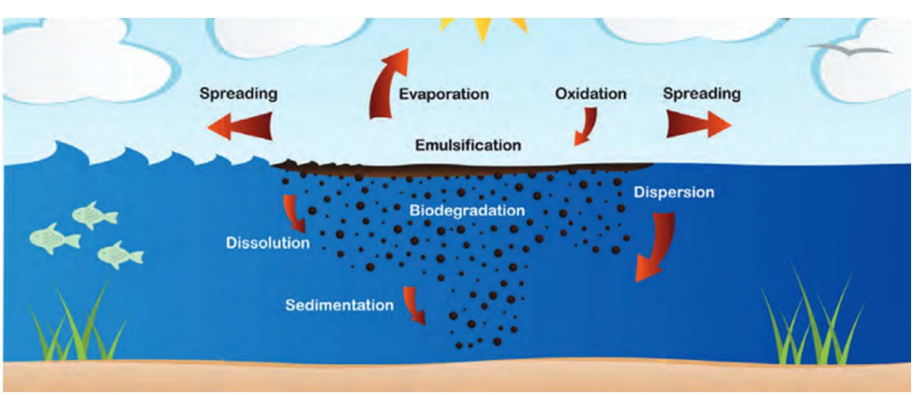

Fig. 1. Sketch showing the processes causing the variation of the composition of the oil film termed weathering.
Source: ITOPF Technical Information Paper: TIP2FateofMarineOilSpills%20(1).pdf, http://www.itopf.com/knowledge-resources/documents-guides/document/tip-2-fate-of-marine-oil-spills, 7 April 2014.

the short-scale surface waves, but also variations in its thickness.

3. Biogenic surface films

Sea surface coverage with biogenic surface films, also called biogenic slicks, is a ubiquitous phenomenon in the World's ocean and is greater than previously thought (Wurl et al., 2011, 2016). On a global scale, the majority of the ocean is not covered with slicks due to low concentrations of organic matter and the dynamics of the sea surface, but in coastal areas the slick coverage is particularly high. The frequency, occurrence, and extent of sea-surface slicks have been studied by Romano (1996) in the eastern Mediterranean Sea, the Red Sea, and the Indian Ocean by taking sea-surface photographs from a ship. This study showed that slicks are observed only at wind speeds below 5 m/s and that slicks occurred with a frequency of 30% in coastal waters and 11% in the open ocean. Biogenic surface films are especially frequently encountered in upwelling areas where the biological activity is high (Clemente-Colon, 2004), in coastal areas during plankton blooms (Lin et al., 2002; Tang et al., 2002), and above coral reefs (Oliver and Willis, 1987). However, there is not a one-to-one correspondence between sea surface coverage with biogenic surface films and high chlorophyll-a concentration. Surface active material of biogenic origin may persist on the sea surface for some time after periods of high biological activity, but it may also drift away from its point of origin due to the action of currents, winds, and waves. The secretion or exudation of surface active material by biota in the water column, which rises to the sea surface, is strongly time-dependent. The composition of biogenic slicks varies with time due to dissolution, evaporation, enzymatic degradation, and photo-catalytic oxidation, which remove selectively constituents from the biogenic slicks. Phytoplankton blooms are usually a yearly recurring phenomenon. For example, a spring plankton bloom occurs in the Baltic Sea every year from March to May (Lin et al., 2003), which gives rise to extensive biogenic slick coverage. Biogenic slicks are also generated by cyanobacteria algal blooms (harmful algal blooms) as encountered often in sea areas and lakes subject to excessive inflow of industrial or agricultural waste water (Wang et al., 2017).

Biogenic surface films can exist on the sea surface only in the form of monolayers, i.e., they are only one molecular layer thick (typically 2.4–2.7 nm). They consist of surface active material (or surfactants) secreted by biota in the water column, including phytoplankton and fish, generally located in the water column below the wave-stirred water layer (Wurl et al., 2016; Kurata et al., 2016). In the presence of waves, the visco-elasticity of the air-sea interface is enhanced causing damping of the short-scale surface waves (Zutic et al., 1981). These films also modify the near-surface turbulence and the air-sea gas exchange. The substances forming the surface films are transported to the sea surface by physical processes including upwelling, turbulence, and rising air bubbles. Under high wind conditions, the upper water layer is filled with air bubbles due to enhanced wave breaking. The bubbles rise to the sea surface and carry with them in their membranes surface active material, which then form biogenic slicks at the sea surface. This is the reason why after high wind speed events coverage of the sea surface with biogenic slicks is particularly high. On the other hand, at high wind speeds, typically above 7–8 m/s, biogenic surface films disappear from the sea surface because they are "washed down" by breaking waves (see, e.g., DiGiacomo and Holt, 2001).

Although the vast majority of monomolecular surface films encountered at sea are of biogenic origin, they sometimes can be of anthropogenic origin. They can originate from waste water spilled into the sea from industrial or urban (sewage) plants (DiGiacomo et al., 2004; Gierach et al., 2017), stormwater runoff from urban environments (Holt et al., 2017) or they can result from bio-degradation of mineral oil films. Thick mineral oil films are often surrounded by monomolecular surface films, which contain very little material, typically only few liters/km^2.

Monomolecular surface films consist of surface active material with molecules having hydrophobic and hydrophilic constituents. The hydrophobic part is directed into the air, while the hydrophilic head group dips into the water layer. This strong interaction with the water causes the molecules to arrange themselves in a monomolecular layer at the air/sea interface. Monomolecular surface films change also the structure of the water layer below the surface down to the thickness of some μm or possibly even down to some hundred μm, in which case this water layer is called vicinial or interfacial water. Although the monomolecular surface films are very thin, they damp the short-scale surface waves (short-gravity/capillary waves) as strongly, or even more strongly, than thick mineral oil films. However, their damping mechanism is different from the one of mineral oil films or emulsions. Due to the action of surface waves, the monomolecular surface film is compressed and dilated, which leads to the generation of (longitudinal) Marangoni waves, which interact with the (transverse) short-scale surface waves and cause the strong damping of the short-scale (transversal) surface waves. For details of this damping mechanism, also called Marangoni damping, the reader is referred to the papers by Alpers and Hühnerfuss (1988, 1989) and Gade et al. (1998a) and the papers quoted therein. The degree of damping of the short surface waves by monomolecular surface films is determined by the complex dilational modulus $E = |E| \exp(-i\theta - \pi)$, which is a function of the dynamic viscosity of the film substance and the surface tension. Marangoni damping is a resonance–type damping. For example, the E-value of oleyl alcohol, which is often used to simulate biogenic slicks, is $|E| = 0.0255$ and $\theta = -175^\circ$. With this value inserted into the Marangoni damping formula (Eq. (1) in Gade et al., 1998a), we obtain maximum damping of 12.8 dB at a frequency of 4.7 Hz. This frequency lies in the frequency range of C-band Bragg waves. Since biogenic slicks should have similar or higher E values than oleyl alcohol, biogenic slicks are expected to be best visible on C-band (frequency around 5 GHz) SAR images, where they generate the highest NRCS contrast. In this radar band, mineral oil films usually generate similar or slightly lower reduction of the radar backscatter than biogenic slicks.

4. Detection of mineral oil films on radar images using conventional methods

In this section we critically review methods that are being applied to detect mineral oil films on radar images. Such images are acquired by real aperture radars (RARs) or synthetic aperture radars (SARs) from airplanes or satellites. Mineral oil spills become visible on radar images as dark areas relative to the surrounding area because they reduce the NRCS. The radar backscattering from clean sea surfaces as well as from surfaces covered with mineral oil and biogenic surface films can be described by the 2-scale Bragg scattering theory (Valenzuela, 1978), which sometimes is also called or composite-surface or tilted Bragg scattering theory. This theory applies for radar backscattering for incidence angles between 23° and at least 50° and for low to moderate wind speeds. At lower incidence angles, specular reflections become important. At higher wind speeds (typically above 8 m/s), non-Bragg scattering processes contribute to radar backscattering due steepening of the waves and wave breaking (Kudryavtsev et al., 2003; Kudryavtsev and Johannessen, 2004). But when the sea surface is covered with surface films, the sea surface becomes smoother and the conditions for the applicability of Bragg scattering theory (Rice, 1951) should be fulfilled even better than for film-free sea surfaces.

Since a key challenge in oil spill detection by radar is the discrimination between oil films and biogenic or monomolecular slicks, we present in the next subsections examples of single-polarization SAR images showing radar signatures of both types of surface films. Conventional methods to discriminate between them are based on the difference in 1) the reduction of the NRCS, 2) position and shape, and 3) texture. In general, position and shape are best suited for discrimination. However, in many cases the radar signatures of both types of surface films are quite similar, which often gives rise to

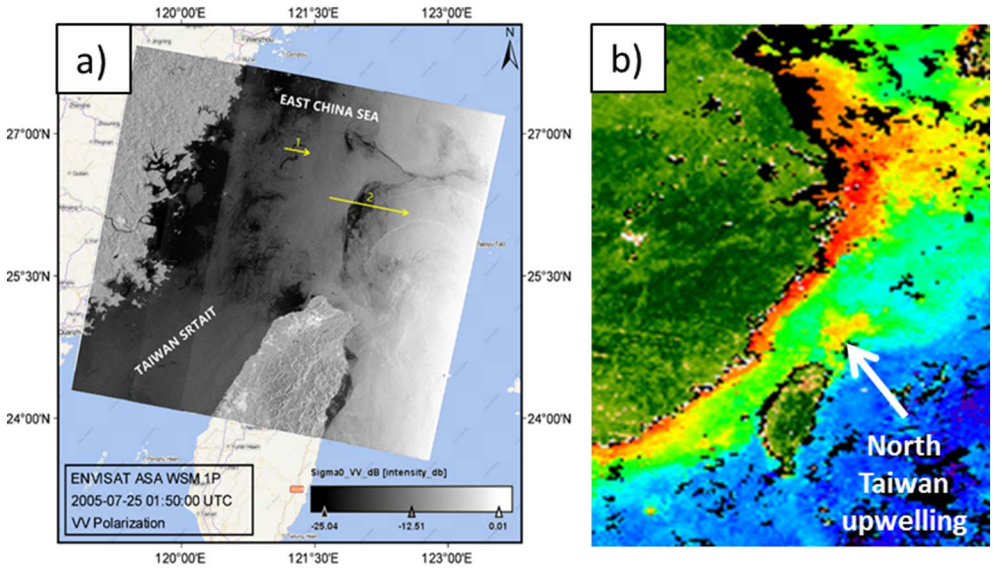

Fig. 3. SAR image acquired by the Advanced SAR (ASAR) onboard the Envisat satellite in the Wide Swath (WS) mode (swath width: 400 km) on 25 July 2005 at 01:54 UTC over the southern East China Sea and the Strait of Taiwan. Visible is in the lower central section the island of Taiwan. The dark patch north of Taiwan and the dark band along the east coast of China are very likely caused by biogenic slicks. (b) Chl-a concentration in July 2005 retrieved from SeaWiFS data showing enhanced Chl-a concentration in an area north of Taiwan and along the east coast of China.

misclassifications.

4.1. Discrimination based on the reduction of the NRCS

The reduction of the radar backscattering from mineral oil films varies considerably depending on 1) the type of oil, 2) time after spillage (during which oil changes temperature and its composition due to weathering), 3) distribution of the oil within the oil patch, and 4) wind speed and direction. Typical values for the reduction of the NRCS by mineral oil films are 5 to 12 dB. For example, Skrunes et al. (2015), using Radarsat-2 data, measured during an oil-on-water exercise in 2012 a reduction of the NRCS of 9.3 dB by crude oil and of 8.3 dB by emulsion (C-band, VV polarization, incidence angle: 35°, wind speed: 6–8 m/s). Biogenic slicks can cause similar or even larger NRCS reductions. For example, Espedal et al. (1998) measured a reduction of 6 to17 dB by the C-band SAR onboard ERS-1, Lin et al. (2002) a reduction of 7.7 dB by the C-band SAR onboard ERS -2, Alpers et al. (2013) a reduction of 10 dB by the C-band SAR onboard Envisat, and Wang et al. (2017) a reduction of 7.3 dB by the C-band SAR onboard Radarsat-2.

Fig. 3a shows examples of biogenic slicks visible on a SAR image, whose likely origins are evidenced by a chlorophyll-a (Chl-a) map. This image was acquired by the Advanced SAR (ASAR) onboard the European satellite Envisat on 25 July 2005 over the southern East China Sea and the Strait of Taiwan. It shows, among others, a dark patch in the upwelling region north of Taiwan, dark areas along the east coast of China and a dark patch at the north western tip of Taiwan. In Fig. 3b the Chl-a concentration is depicted for July 2005, which was retrieved from data of the Sea Wide Field-of-view Sensor (SeaWiFS) onboard the OrbView-2 satellite. It shows enhanced Chl-a concentration in an area north of Taiwan and along the east coast of China (Tang et al., 2002). By comparing the SAR image with the Chl-a map, one can see that the dark areas north of Taiwan and along the east coast of China correlate well with areas of enhanced Chl-a concentration. The dark patch at the north western tip of Taiwan is very likely also caused by biogenic slicks, since the weekly Chl-a map (from 25 July to 2 August 2005).

August 2005) retrieved from data of the Moderate Resolution Imaging Spectrometer (MODIS) (not reproduced here) shows enhanced Chl-a concentration also in this region. This Chl-a enhancement is probably caused by eutrophication of the coastal waters by nutrients transported into the sea by the Taipei River. Also visible on the SAR image depicted in Fig. 3a are two dark patches adjacent to the east coast of Taiwan. They are very likely not caused by mineral oil, but by surface active material associated with waste water from industrial or urban (sewage) plants transported by rivers into the sea.

Visible is on the SAR image is also a curved dark band in the northern central section of the image (labeled “1”), which we interpret as being caused by a mineral oil spill.

We have made NRCS scans through several dark areas visible on the SAR image (Fig. 3a) and have depicted two of them in Fig. 4: one through the oil spill (line 1) and the other through the slick (upwelling)

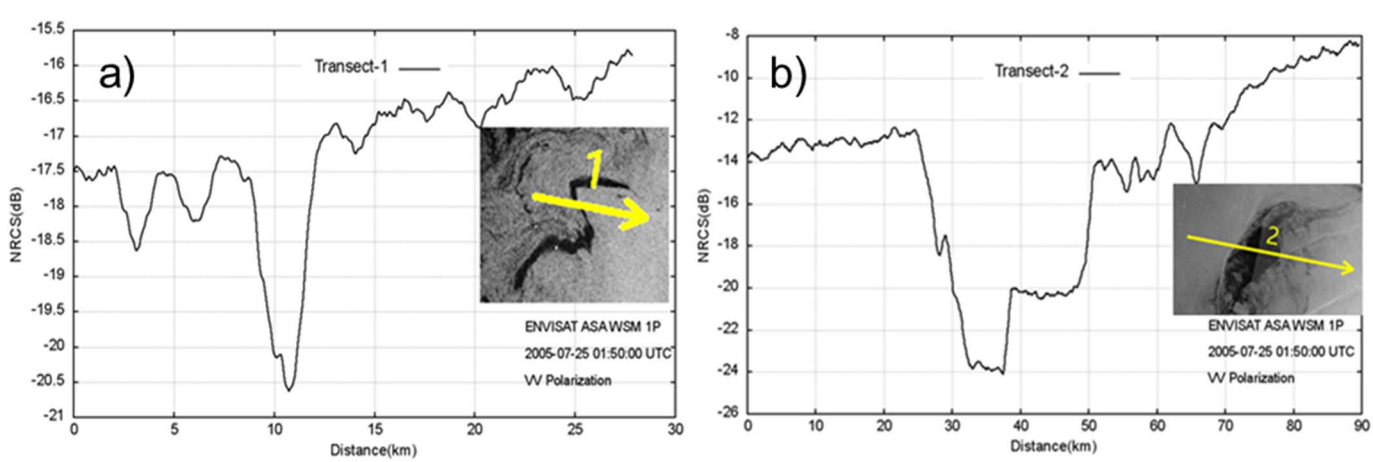

Fig. 4. (a) NRCS scans through radar signatures of an oil spill (line 1) and (b) the biogenic slick in the upwelling area north of Taiwan (line 2).

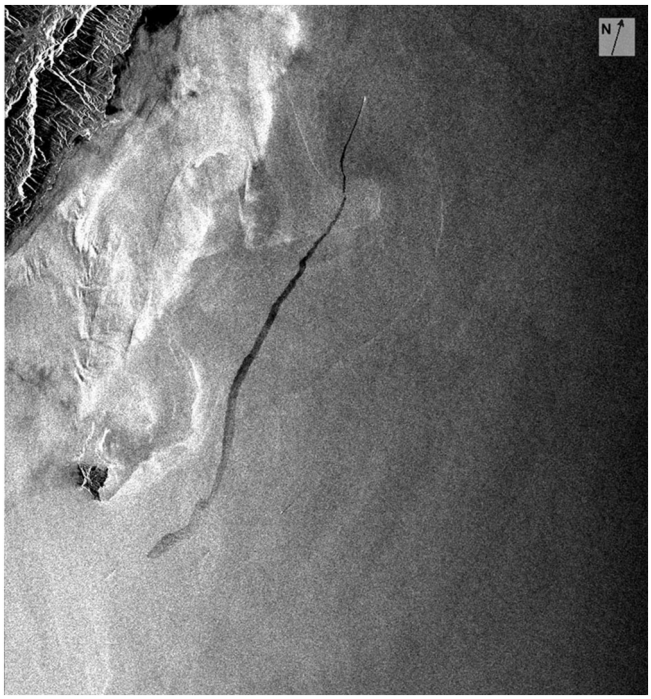

Fig. 5. SAR image acquired by the ERS-1 satellite on 20 May 1994 at 14:20 UTC over the Pacific Ocean east of Taiwan (frame center: 23° 01′N, 121° 41′E) showing an oil spill trailing a ship (the bright spot at the front of the black line). The oil disperses with time causing the oil trail to widen. Imaged area: 100 km × 100 km.

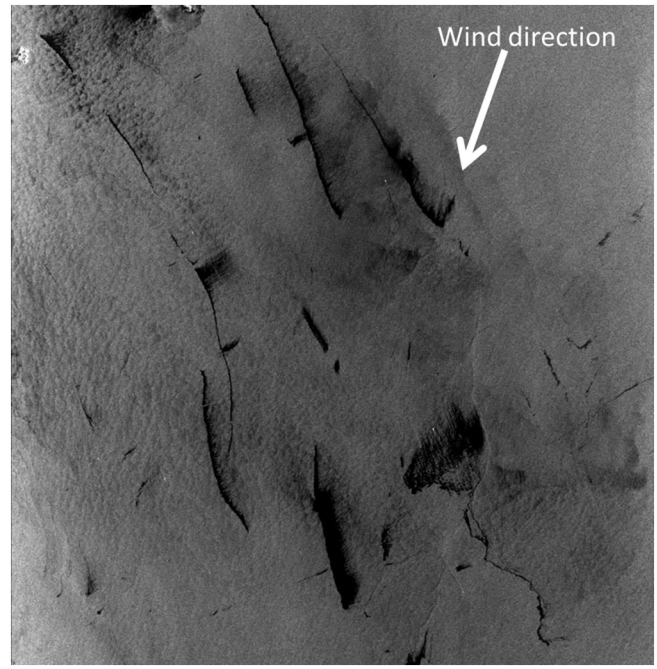

Fig. 6. SAR image acquired by the European Remote Sensing satellite ERS-2 on 4 April 1997 at 3:25 UTC over the South China Sea (frame center: 4° 20′N, 103° 59′E) showing a massively oil polluted sea area off the coast of Malaysia (off Kuantan) which is a busy shipping lane. The wind blew from a northeasterly direction causing the feathering of some of the larger oil trails. Imaged area: 100 km × 100 km.

area north of Taiwan (line 2). They show that the mineral oil films reduces the NRCS by only 3 dB, while the biogenic slick reduces it by 10 dB. Also the reduction of the NRCS by the two dark patches at the east coast of Taiwan was measured to be 11 dB and 12 dB, respectively. Thus, surface films not being mineral oil films can cause quite strong NRCS reductions and should not be called weakly damping surface films as often done in the literature. These examples clearly demonstrate that it is not feasible to base discrimination algorithms on differences in the reduction of the NRCS, since both types of surface films give rise to comparable NRCS reductions.

4.2. Discrimination based on differences in position and shape

Identifying oil films by the position/shape of the dark areas is the most viable method. It is possible, for example, 1) when a dark line is located behind a ship visible on a SAR image as a bright spot (Fig. 5), 2) when a linear dark feature broadens from one end to the other (Fig. 3a and Fig. 5) or 3) when the dark patch has a feathered shape (Fig. 6). The broadening of the linear feature is due to lateral diffusion which increases with time after spillage. The feathered shape is a consequence of the fact that the wind has a stronger grip on the heavier components of the oil film and thus these components are moved faster by the wind than the lighter components. Thus, the downwind side of mineral oil films usually have sharp boundaries. Biogenic slicks cannot have such feathered shapes because of their monomolecular structure. Oil originating from oil seeps (natural seepages from a hydrocarbon reserves) or oil platforms/oil terminals can often be detected by using time series of SAR images. The oil films manifest themselves as recurring features at the same location (Espedal and Wahl, 1999; Suresh et al., 2015). MacDonald et al. (2015) have used this approach to map the extensive natural seeps in the Gulf of Mexico.

Most often, biogenic slicks form connected, homogeneous slicks as visible on the SAR image acquired by the European Remote Sensing satellite ERS-1 over the upwelling area north of Taiwan on 23 July 1994 (Fig. 7a). The large dark patch is located in the upwelling area as evidenced by the lower sea surface temperature (SST) values relative to the surrounding area (Fig. 7b). In upwelling areas, cold water carrying nutrients is transported from lower levels to the sea surface causing a plankton bloom in the near-surface water layers (euphotic zone).

While sometimes mineral oil films can be identified on SAR images unambiguously by their position and shape, like on the SAR images depicted in Figs. 5 and 6, this is not generally the case. Given the position and shape, some uncertainty always remains. An example showing this is depicted in Fig. 8a, which shows in the lower right hand section a dark pattern consisting of 4 curved dark lines that seem to emanate from one point (see also the zoom on this pattern depicted in Fig. 8b). We have checked the sea chart for positions of oil platforms in this area, but found no oil platform at this position. Thus, we suspect that the pattern originates from an oil seep, but we cannot be sure since the sea chart, which we used for locating oil platforms, may not have been up-to-date at the time of the SAR data acquisition. This SAR image shows further two oil spill look-alikes: two rain bands and a low wind speed area. We are certain that the two strings of bright and dark patches stretching perpendicular to the coast line into the sea are sea surface signatures of rain cells aligned in a rain band since the weather radar image of the Hong Kong Observatory (not reproduced here) shows two rain bands at these positions. As shown by Alpers et al. (2016), C-band radar signatures of rain cells usually consist of areas of enhanced and reduced radar backscatter relative to the background. Enhancement of the NRCS is caused by downdraft winds and scattering from ring waves and splash products (stalks and craters) generated by the rain drops impinging onto the sea surface. Reduction is caused by the attenuation of the short surface waves (the Bragg waves) by turbulence generated by in the upper water layer by the impinging rain drops. However, we cannot exclude completely that some dark patches within the rain bands result from mineral oil films. Oil could have accumulated there due the local winds associated with the rain band. Concerning the large dark area west of the dark oil seep pattern, we suspect that it is caused by low winds. We have checked the sea surface wind field as given by National Centers for Environmental Prediction (NCEP) and found that in this area the wind speed at 03:00 UTC was

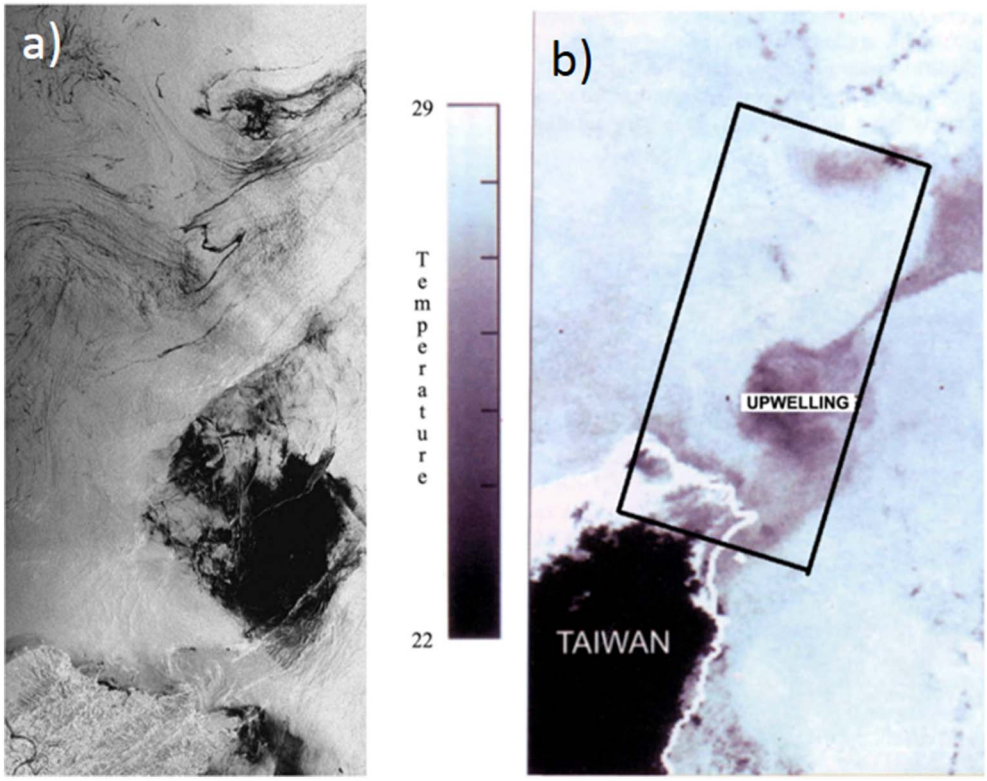

Fig. 7. (a) SAR image acquired by the European Remote Sensing satellite ERS-1 on 23 July 1994 at 02:26 UTC over the upwelling area north of Taiwan. (b) SST image (in degrees Celsius) acquired by the Advanced Very High Resolution Radiometer (AVHRR) onboard the NOAA-11 satellite on 22 July 1994 at 08:03 UTC showing the upwelling area as an area of low SST.
Source: Clemente-Colon (2004). Area imaged by SAR: 100 km × 200 km.

between 2 and 4 m/s, which is around the threshold for surface ripple generation. Furthermore, also the wind direction was changing in this area at that time. Thus, it is very likely that in this area no Bragg waves were generated by the wind such that there was no radar backscatter. The SAR image depicted in Fig. 8a is typical for many other similar SAR images, on which oil spills and oil spill look-alikes cannot be determined unambiguously. The level of confidence for identifying oil spills on SAR images depends strongly on the expert knowledge of the image interpreter. The more auxiliary information is available, the higher will be the level of confidence for identifying oil spills.

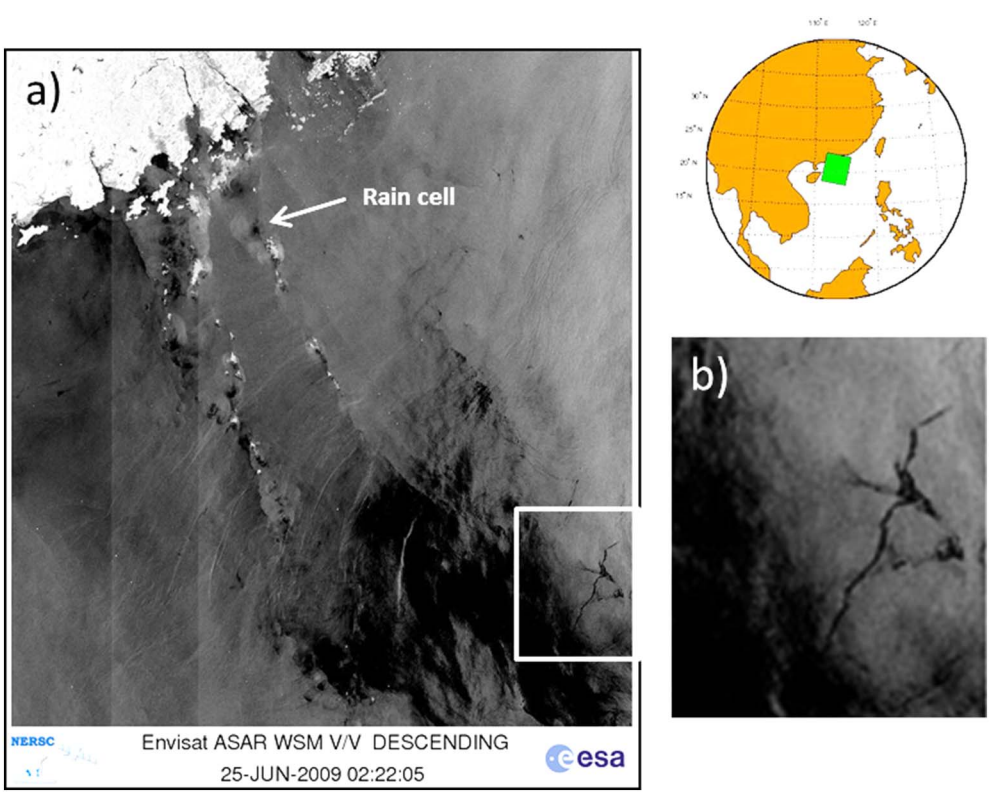

Fig. 8. (a) SAR image acquired by ASAR onboard the Envisat satellite on 25 June 2009 at 02:22 UTC over the South China Sea southwest of Hong Kong, see attached map. (b) Zoom on the pattern marked by a rectangle in (a), which, very likely, is the radar signature of a mineral oil film associated with an oil seep. Visible are also radar signatures of two rain bands consisting of a string of bright and dark patches. The white arrow points to a typical radar signature of a rain cell, consisting of a dark patch surrounded by a bright area caused by downdraft winds. The bright line within the large dark area is the radar signature of an internal solitary wave originating from the Luzon Strait. Imaged area: 400 km × 405 km.

Fig. 9. SAR image acquired by ERS-1 satellite on 16 April 1994 at 21:04 UTC over the Baltic Sea (Pommerian Bight). Visible is in the lower left hand section the German island of Ruegen and on the top the Swedish coast. This SAR image shows biogenic slicks entrained by a complex surface current field. The dark area to the left is very likely an area completely covered by biogenic slicks. Note also in the upper left hand section the dark line with a bright spot at the end where the line is narrowest (to the right). It clearly results from oil spilled from a ship. Imaged area: 100 km × 100 km.

4.3. Discrimination based differences in texture

Due to the physico-chemical properties of surface active material forming biogenic slicks, surface active materials has the tendency to form contiguous, homogeneous surface films. This property was observed during the SIR-C/X-SAR experiment in the North Sea in 1994 during which several kinds of surface active material, among them oleyl alcohol, were laid onto the sea surface (Gade et al., 1998b). During this experiment, frozen chunks (typically 100 g) of surface active materials were thrown from a helicopter onto the sea. After melting, the films emanating from each chunk quickly combined to form a large, connected, homogeneous, monomolecular surface film. However, when the amount of surface active material is limited, then it can also form inhomogeneous slick areas. The surface currents can gather up and entrain surface active material in convergent regions of the surface current field. Thus, biogenic slicks often serve as tracers for small-scale current features, like small-scale eddies, and thus make them visible on SAR images (see, e.g., DiGiacomo and Holt, 2001; Munk et al., 2000; Munk, 2001; Karimova, 2012; Alpers, 2014). An example of a SAR image showing entrainment of slick material in a surface current field is depicted in Fig. 9. This SAR image was acquired over the Baltic Sea during the time of the spring plankton bloom when much surface-active material is secreted by the biota in the water column giving rise to large biogenic slick coverage.

Mineral oil form connected oil films immediately after spillage, but then, after some time, they break into patches as shown in Fig. 10. This SAR image was acquired over the Yellow Sea approximately 5 days after a large amount of crude oil was spilled from a tanker following a collision with another ship (Kim et al., 2015). The oil spread from the point of collision to the south due to the action of the wind and currents (mainly tidal currents). Like surface active material of biological origin, also mineral oil can be entrained by surface currents. Thus, we conclude that also texture cannot always be used as a reliable indicator for discriminating between mineral oil films and biogenic slicks.

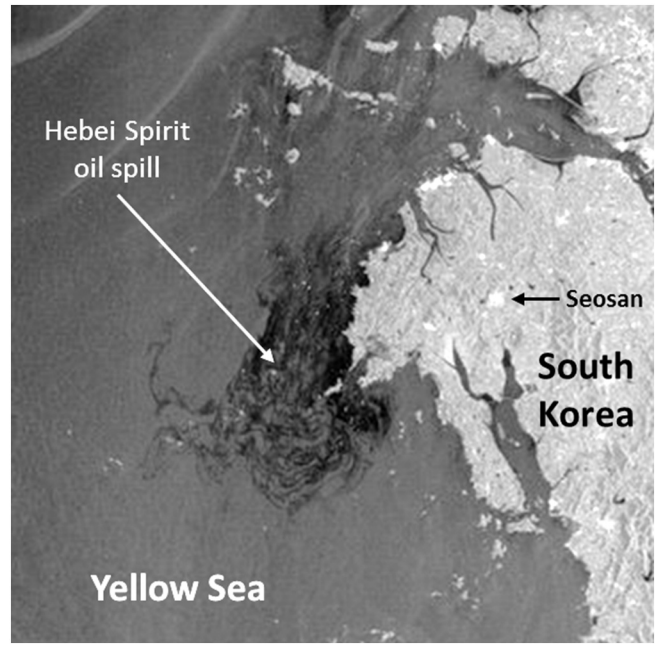

Fig. 10. SAR image acquired by the ASAR onboard the Envisat satellite on 11 December 2007 at 01:40 UTC over the Yellow Sea showing the crude oil spill from the tanker Hebei Spirit after it had collided with a towed crane barge on 6 December 2007 at 22:15 UTC off the coast of South Korea (126.05°E, 36.86°N). Note that the oil film has broken up into patches and has probably formed emulsions. Imaged area: 200 km × 200 km.

5. Detection of mineral oil films using statistical properties of the radar backscatter

In this section we discuss methods which have been proposed to discriminate between mineral oil films and biogenic (monomolecular) surface films that are based on differences in the statistical properties of the radar backscatter. The first method uses single-polarization SAR data (Section 5.1) and the second one dual-polarization SAR data (Section 5.2).

As discussed in Sections 2 and 3, biogenic and mineral oil surface films have quite different physico-chemical properties which should result in differences in the statistical behavior of the radar backscatter. However, extracting geophysical information from variations of the image intensity within a SAR scene is not as straightforward as from optical images, where statistical properties have been quite useful in classifying imaged objects. In the case of SAR images, this is more complex because of speckle, which results from the fact that SAR employs coherent signals to generate images. The SAR images have "salt and pepper" appearance caused by constructive and destructive interferences between the radar backscattering from a large number of elementary scatter elements within a resolution cell. When their number is sufficiently large and the target scene is homogeneous, then the central limit theorem applies in which case the phase of backscattered signal from a resolution cell is uniformly distributed, its modulus is Rayleigh- distributed, the real and imaginary parts of the scattering amplitude are identically Gaussian- distributed, and the intensity, i.e., the square of the modulus of the scattering amplitude, is negative exponentially distributed (Ulaby and Dobson, 1987). While the mean value of the scattering amplitude contains information on the target, the phase, which is uniformly distributed between $-\pi$ and $+\pi$, does not contain such information. However, as we shall show in Section 5.2, that the co-polarized phase difference (CPD) does contain information on target properties and could therefore be used for target discrimination purposes. The CPD is defined as $\phi_c = \phi_{HH} - \phi_{VV}$, where ϕ_{ij} denotes the phase of the received electric field for the receive polarization i and for the transmit polarization j. The subscripts H and V

refer to horizontal and vertical polarizations, respectively.

However, when the imaged scene is small and inhomogeneous, then the central limit theorem does not apply and the modulus of the backscattered radar signal may not be Rayleigh distributed and the phase not uniformly distributed. In the case of "non-fully developed speckle statistics" the level of pixel-to-pixel variation is higher than in the fully developed speckle case. In order to reduce the pixel-to-pixel variation, multi-looking techniques are often applied. But this leads to a reduction in spatial resolution, which makes it even harder to extract physico-chemical properties from small areas of differing radar backscatter (e.g., from small oil patches).

Radar backscatter from the rough sea surface does not follow Gaussian statistics, which was noted > 40 years ago by Jakeman and Pusey (1976). These authors attributed the deviation from Gaussian statistics to the presence of long ocean waves and wave breaking. Consequently, researchers have tried to use other probability distribution functions which are more suitable to model the statistics of the radar backscattering from the sea surface. One option is the three-parameter generalized K-probability density function, which Migliaccio et al. (2007) used in their analysis of SAR images. They analyzed several single-look complex C-band (VV polarization) SAR images acquired by the European Remote Sensing satellites ERS-1 and ERS-2 at VV polarization over European waters showing radar signatures of (supposedly) mineral oil films. They found differences in the parameters of this distribution for oil-covered and oil-free surfaces. However, discrimination among oil spills and other dark regions visible on SAR images was not possible.

5.1. Discrimination based on differences in the statistics of the image intensity

Skrunes et al. (2014) applied a product model for the description of the statistics of the image intensity (I) by writing it as the product of two random variables, $I = \tau \cdot X$, where τ describes the variation of the SAR image intensity due the physical processes (texture) and X the variation due to speckle, which they assumed to have a negative exponential distribution, i.e., it is describable by Gaussian statistics. They analyzed the SAR image intensity in terms of "log cumulants" and generated "log-cumulant diagrams". In their statistical analysis they used Radarsat-2 and TerraSAR-X images, which were acquired during two large-scale oil-on-water exercises in the North Sea in 2011 and 2012 during which crude oil, oil emulsion, and plant oil were put onto the sea surface. They found significant differences in the log-cumulants from areas covered with mineral and from adjacent oil-free areas as well as from areas covered with plant oil. They concluded from these differences that radar backscattering from mineral oil films is more inhomogeneous than from plant oil films. This interpretation is in accordance with our interpretation of the statistical behavior of dual-polarization data, see next subsection. However, the results obtained by Skrunes et al. (2014) could have been affected (contaminated) by non-fully developed speckle statistics due to the small size of the oil patches.

5.2. Discrimination based on differences in the statistics of the co-polarized phase difference

It has long been recognized that in land applications that the co-polarized phase difference (CPD) is a valuable discriminator for terrain classification. The CPD depends on sensor as well as on target parameters. Its statistical properties vary with radar wavelength, incidence angle, surface roughness, and type of vegetation cover, vegetation geometry, and biophysical properties of the land targets (Ulaby et al., 1992; Lee and Pottier, 2009, and the references quoted therein). In addition, the CPD is also sensitive to inhomogeneity of the imaged scene (see, e.g., Haldar et al., 2014). Inhomogeneity causes a reduction of the coherence between the two polarized phases and thus causes a broadening of the probability density function (PDF) of the CPD or an increase of the standard deviation (STD).

Migliaccio et al. (2009) have proposed to use the STD of CPD for discriminating between sea surfaces covered with mineral oil films and biogenic slicks. They have applied this method to radar backscattering from the sea surface and shown that the STD of the CPD is much larger for sea surfaces covered with mineral oil films than for oil-free sea surfaces and sea surfaces covered with artificial monomolecular surface films. They obtained this result from the analysis of SAR data acquired by the C-band SAR onboard the Spaceshuttle during the SIR-C/X-SAR mission in 1994 and by the Phased Array L-band SAR (PALSAR) onboard the first Japanese Advanced Land Observing Satellite (ALOS-1). The first data set was acquired during a campaign carried out by the University of Hamburg in the North Sea during which mineral oil films and monomolecular surface films of different chemical compositions were put onto the sea surface (for details see Gade et al., 1998b). The second data set was acquired over various sea areas showing radar signatures of mineral oil films (but not verified). They concluded that the large measured STD of the CPD for radar backscattering from mineral oil films is caused by a non-Bragg scattering mechanism. Zhang et al. (2011) arrived at the same conclusion by computing the conformity parameter from Radarsat-2 data over the Gulf of Mexico. Skrunes et al. (2014) arrived also at this conclusion by computing the real part of the cross-polarization correlation function and the geometric intensity (the combined intensity in the co-polarization channels) from Radarsat-2 data acquired during an oil spill exercise in the North Sea in 2011 and 2012, which involved crude oil, emulsion, and plant oil.

However, we challenge the interpretation that the large STD of the CPD obtained from radar backscattering from mineral oil films is caused by another scattering mechanism than Bragg scattering. Instead, we attribute it (assuming that the data are not contaminated by instrument noise) to fluctuations of the radar backscatter due to inhomogeneity of scattering medium. Our arguments are as follows:

It is well known that from land applications, that the CPD contains information on the scattering mechanism and on the physical properties of the scattering target (roughness, dielectric constant, and geometry). The statistical property of the CPD is characterized by the PDF, which, in the case of surface scattering, has a Gaussian shape and is characterized by its mean and the standard deviation (Ulaby and Dobson, 1987). As mentioned before, radar backscattering from a moderately rough sea surface with no long waves present, can be described, at intermediate incidence angles, by Bragg scattering theory (Rice, 1951; Valenzuela, 1978). For Bragg scattering, there is no phase shift between the backscattered signals at HH and VV polarizations. Therefore, for a homogeneous sea surface with no long waves present, the PDF of the CPD should, theoretically, be a delta function centered at zero degree. However, due to instrument noise, it is always somewhat broadened. When long waves are present, the PDF is further broadened due to the fact that the Bragg waves are tilted by long waves. Tilting causes variations of the radar backscatter since the NRCS depends on the local incidence angle, and this dependence is polarization-dependent. The rougher the sea, the broader is the PDF of the CPD.

However, broadening can also be caused by inhomogeneity of the scattering medium, which, in the case of scattering from mineral oil films or emulsions, can be caused by irregular patches of differing radar backscatter due to variations of the thickness of the oil layer or due to variations of the dielectric constant. The latter effect can occur only when the mineral oil layer is sufficiently thick or when the emulsion layer has a structure such that the radar beam can sense the relative dielectric constant of the oil, see Section 6. Although the increase of the STD of the CPD due to inhomogeneity of the scattering medium is a commonly observed phenomenon in scattering from land targets, its theoretical explanation is not straightforward. Ulaby et al. (1992) state: "At present, we are still in the early stage of developing an understanding of scattering by inhomogeneous media, particularly with regard to the statistics of the co-polarized phase angle". One way to

explain the broadening of the PDF of the CPD is to associate it with non-fully developed speckle statistics caused by the inhomogeneity of the scattering medium and the small size of the oil patches. As stated before, non-fully developed speckle statistics leads always to larger of pixel-to-pixel variations and thus to a broadening of the PDF.

Another effect that also contributes to the broadening of the PDF of the CPD is caused by the fact, that polarimetric SARs (usually) transmit V and H polarization signals successively, i.e., with a time delay between the transmissions. The movement of the SAR between successive transmissions at V and the H polarizations causes decorrelation between the two received signals since they do not view exactly the same area on the sea surface. For sea surfaces covered with inhomogeneous mineral oil films, the decorrelation will be larger than for sea surfaces covered with homogeneous monomolecular slicks. Thus, we conclude that inhomogeneous Bragg scatter from mineral oil films could explain the observed broadening of the PDF of the CPD and thus there is no need to invoke non-Bragg scattering to explain this effect.

In the case of emulsions, similar arguments apply: The broadening could be explained by the combined effect of variations of the radar backscatter caused by wave damping and of variations of the dielectric constant due to variations of the oil/water mixing ratio in the emulsion layer. Another argument in favor of our hypothesis that Bragg scattering applies also for scattering from mineral oil films is based on the shape and mean value of the PDF of the CPD. Scattering theory predicts that for single-bounce scattering at smooth dielectric surfaces, the PDF of the CPD has a Gaussian shape centered at zero degrees, but for a double-bounce (dihedral) scattering it is centered at 180°. For mixed scattering, which is applicable for most natural targets, the mean value of the CPD lies between 0 and +/−180°. For example, Ulaby et al. (1987) have shown that the mean value of the CPD for radar backscattering at L-band from a corn field is quite large due to scattering at the stalks of the corn plants. But for radar backscattering from (slightly rough) bare soil or cut vegetation, the PDF is centered close to zero degree and has a Gaussian shape. This last scattering resembles scattering from slightly rough sea surfaces.

6. Detection of mineral oil films using differences in the dielectric constant

The fact that Bragg scattering depends on the dielectric constant of the scattering layer and that the scattering is polarization-dependent, offers the possibility to discriminate between mineral oil films/emulsions and biogenic slicks by exploiting the difference in the radar backscatter at HH and VV polarizations as proposed by Minchew et al. (2012). However, this method only works, when the oil film is sufficiently thick or the emulsion layer has a structure such that the radar beam can sense the relative dielectric constant of the oil-water mixture. The radar signal penetrates into the water body only to a depth, that is characterized by the e-folding depth δ, which is determined by the radar wavelength (λ) and the imaginary part (Im) of the relative dielectric constant (ε_r) of water:

$$\delta = \lambda\,(4\pi)^{-1}\ (\mathrm{Im}\ \ \varepsilon_r)^{-1/2} \tag{1}$$

Inserting the value ε_r for sea water, $\varepsilon_r = 60 - j\ 35$ (assuming a salinity of 32.54 psu and a water temperature of 10 °C) and a radar wavelength of $\lambda = 5.6$ cm (C-band), we obtain $\delta = 0.4$ cm (Skrunes et al., 2015). For the dielectric constant to have a non- negligible influence on the radar scattering, the oil layer must have a thickness exceeding 1/10 of the penetration depth. In the case of a C-band SAR, the oil layer must be thicker than 1 mm and in the case of the L-band SAR thicker than 4 mm (Franceschetti et al., 2002).

Since mineral oil has a very low dielectric constant (a typical value is $\varepsilon = 2.3 - j\ 0.02$, see Minchew et al., 2012), oil entrained in water changes the dielectric constant considerably, which opens up the possibility to measure the oil-water mixing ratio as discussed by Minchew (2012). In the case of mineral oil rising to the surface from natural seeps, or, as in the case of the "Deepwater Horizon" accident from a well integrity failure of an oil rig, the emulsion layers could be thicker than the ones originating from oil spills. According to electromagnetic scattering theory the NRCS (σ^o_{ij}) for scattering from the rough ocean surface is, to first order, given by (Valenzuela, 1978):

$$\sigma^o{}_{ij} = 4\pi k^4\ \cos^4\theta_i\ |R_{ij}(\theta)|^2 E(2k\sin\theta_i, 0) \tag{2}$$

where $k = 2\pi / \lambda$ is the wavenumber of the electromagnetic radiation, θ_i is the incidence angle, $E(k_x, k_y)$ is the two-dimensional (Cartesian) wave-number spectral density of the sea surface roughness, and R_{ij} are the first-order scattering coefficients. The indices i, j denote the polarization of the incident and back-scattered radiation, respectively. The incident beam is in the x-z plane (z is the vertical direction and x, y are the horizontal coordinates). For VV polarization, R_{ij} reads

$$R_{VV} = \frac{(\varepsilon_r - 1)\{\sin^2(\theta_i) - \varepsilon_r[1 + \sin^2(\theta_i)]\}}{(\varepsilon_r\cos(\theta_i) + \sqrt{\varepsilon_r - \sin^2(\theta_i)})^2}. \tag{3}$$

and for HH polarization it reads

$$R_{HH} = \frac{\cos(\theta_i) - \sqrt{\varepsilon_r - \sin^2(\theta_i)}}{\cos(\theta_i) + \sqrt{\varepsilon_r - \sin^2(\theta_i)}} \tag{4}$$

Formulas (2), (3), and (4) are the basic formulas of Bragg scattering theory. Note that in the case of thick oil films or emulsion layers, the reduction of the NRCS is due to two mechanisms: 1) the damping of the wind-generated Bragg waves by the mineral oil and 2) the reduction of the dielectric constant of the ocean surface layer due to the mineral oil. The simplest way to measure differences in the dielectric constant would be to measure the co-polarized NRCS ratio, $\sigma^o_{HH}/\sigma^o_{VV}$. This ratio is, to first order (in the absence of long waves), independent of the ocean wave spectrum $E(2k\sin\theta_i,0)$ and depends only on the scattering coefficients for VV and HH polarizations, which are functions of the effective dielectric constant ε_{eff} of the scattering medium and of the incidence angle (see Eqs. (2)–(4)):

$$\sigma^o{}_{HH}/\sigma^o{}_{VV} = R_{HH}/R_{VV} \tag{5}$$

This ratio is identical for scattering at clean sea surfaces and sea surfaces covered with biogenic slicks, because the radar does not sense the dielectric constant of monomolecular surface films due to its very thin thickness (Gade et al., 1998a). However, for thick oil films or emulsions, the dielectric constant of oil affects the radar backscattering and thus also the co-polarized NRCS ratio. When long waves are present, Eq. (5) has to be modified and the two-scale Bragg model must be applied. Thus the ratio $\sigma^o_{HH}/\sigma^o_{VV}$ can be used to discriminate between thick mineral films/emulsion layers and biogenic slicks because this ratio is different for the two kinds of surface films. Note that in the case of biogenic slicks the dielectric constant of the biogenic slick material does not enter into the radar backscattering mechanism because biogenic surface films are extremely thin.

Based on copolarized SAR data, Minchew et al. (2012) and Minchew (2012) have developed a method to retrieve oil/water mixing ratio by exploiting the dependence of Bragg scattering on the effective dielectric constant of the emulsion layer. They used in their investigation SAR data acquired by the low-noise UAVSAR over the former site of the Deepwater Horizon (DWH) drilling rig and showed that most of the oil near the DWH was mixed with sea water to a minimum depth of a few millimeters. The data also show that, in the incidence angle range between 26° and 60°, radar backscatter from both the oil covered and the clean water area is dominated by surface scattering, which is consistent with the two-scale Bragg scattering theory (Minchew et al., 2012).

7. Detection of mineral oil films using polarimetric parameters

Polarimetric parameters derived from fully-polarimetric or quad-polarimetric SAR data have been used quite successfully in land applications to determine the scattering mechanisms causing observed

radar signatures, like Bragg scattering and multiple scattering (Zebker and van Zyl, 1991; Cloude and Pottier, 1996). Several polarimetric parameters have been derived from the scattering matrix, with the widely used parameters being the entropy (H), the anisotropy (A), and the mean scattering angle (α). A large number of papers have been published in the last decade dealing with SAR polarimetry for oil spill detection (for a review, see, e.g., Migliaccio et al., 2015) in which it is claimed that SAR polarimetry is also beneficial for discriminating between mineral oil films and biogenic slicks. In these papers, it is shown that certain polarimetric parameters exhibit differences in radar backscattering from mineral oil films and biogenic slicks (and clean sea surfaces) and most authors attribute the difference to the fact that for radar backscattering from mineral oil films cannot be described by Bragg-scattering theory. For example, Migliaccio et al. (2009) inferred this from the large value of the standard deviation of the co-polarized phase difference (CPD) measured over mineral oil films, Velotto et al. (2011) inferred it from the low correlation between HH and VV radar backscatter, Zhang et al. (2011) from the negative value of the conformity parameter and the large value of the polarimetric entropy, Skrunes et al. (2014) from the low value of the real part of the copolarization cross product, and Li et al. (2015) from the positive value of the ellipticity parameter and the low degree of polarization.

While Migliaccio et al. (2009) and Nunziata et al. (2008) did not specify what kind of scattering mechanism causes non-Bragg scattering from mineral oil films, Zhang et al. (2011) and Li et al. (2015) attribute it to double-bounce or dihedral scattering, and Skrunes et al. (2015) to suppression of the non-polarized (NP) radar backscatter. However, we are not convinced that measured differences in the radar backscatter from sea surfaces covered with mineral oil films and biogenic slicks (and from clean sea surfaces) are caused by non-Bragg scattering. Instead, we hypothesize that the measured differences are mainly caused by instrument noise and not by physical processes. The strongest support of this hypothesis comes from Minchew et al. (2012) who carried out measurements over the Gulf of Mexico with the UAVSAR, which has an extremely low noise floor of − 53 dB. Minchew et al. (2012) state in their paper, that "L-band radar backscatter from both oil and water in moderate wind conditions are well described by the tilted Bragg model across the range of incidence angles from 26° to 60°, with the backscatter from oil being even more strongly governed by surface scattering from a single dominant scatter than backscatter from water for incidence angles below 50°."

Arguments against the hypothesis that the non-Bragg scattering part of the scattering mechanism is double-bounce or dihedral scattering (Zhang et al., 2011; Li et al., 2015) can be found in Plant et al. (2010). These authors have studied extensively double-bounce scattering theoretically and concluded that this type of scattering does not contribute to radar backscattering at VV polarization up to incidence angles of 89°, but it does contribute to radar backscattering at HH polarization when the waves break and when the incidence angle is above 45°. However, the Radarsat-2 quad-polarization SAR data analyzed by Zhang et al. (2011) do not fulfill these requirements, since in their case the incidence was between 41.9° and 43.4° and the wind speed was 6.5 m/s, where wave breaking should have been small. Furthermore, we suspect that their data may have been affected by instrument noise because of the high incidence angles. Note that in the calculation of the conformity parameter cross-polarization data are used, which are particularly prone to signal-to noise problems.

Using also Radarsat-2 data, Li et al. (2015) obtained the result that, in the case of scattering from an oil film originating from the DWH accident (and also for scattering from oil-free sea surfaces), Bragg scattering applies, while in the case of scattering from oil films originating from natural oil seeps, double-bounce or even-bounce scattering applies. They arrived at this result by simulating hybrid-polarimetric SAR data from Radarsat-2 quad-polarimetric SAR data and then calculated the ellipticity parameter chi (χ) and the degree of polarization (m). The sign of χ is an indicator for even versus odd bounce backscatter. While Bragg scattering is single-bounce scattering, which reverses the sense of the circular rotation of the incoming radar beam, dihedral scattering (scattering from two inclined planes) is double-bounce scattering, which does not reverse the sense of the circular rotation. Li et al. (2015) have presented a plot (Fig. 2e) which shows that in the case of radar backscattering from a mineral oil film originating from an oil seep the sign of χ is positive indicating even-bounce (or double bounce) scattering. They argue that the reason for this is that mineral oil layer give rise to multiple reflections and volumetric backscattering. However, multiple reflections can only occur when the thickness of the oil layer is of the order the radar wavelength (i.e., several centimeters) or larger, which, in general, is not the case. We suspect that the positive sign of χ is an artifact caused by instrument noise and not by a physical effect, i.e., not by double-bounce or even-bounce scattering. This supposition is supported by the observation that the oil seep data were acquired at relatively high incidence angles (between 41.9° and 43.4°), while the DWH data were acquired at low incidence angles (between 29.2° and 30.9°). Since the signal-to noise (S/N) ratio strongly decreases with incidence angle, the oil seep data should be much more prone to noise contamination than the DWH data. Note also, that cross-polarization quad-polarimetric data, which are particularly sensitive to signal-to noise problems, enter into the calculation of χ (Raney, 2007, 2016).

However, we acknowledge that non-Bragg scattering caused by non-polarized (NP) scattering at breaking waves is a real effect and that NP scattering is modified by surface films. This was also shown by Skrunes et al. (2015) by analyzing Radarsat- 2 and TerraSAR (X-band) SAR data. In a recent study (Hansen et al., 2016) it was suggested that the reduction of NP scattering by surface films has the potential to be used for discriminating between different film types of surface films. Understanding how breaking waves impact the spreading, distribution, and possible changes of the physical properties of oil slicks, is a very challenging task and requires unique validation methods as well.

8. Experience with validation of mineral oil films detected on radar images

Developers of oil spill detection algorithms using SAR data usually train and validate their algorithms using "soft data", i.e., the dark features visible on the SAR images have usually not been validated and the classification has been based on subjective interpretation. Thus the claim made by many investigators that their algorithm has a high success rate (few false alarms) has to be taken with care. Even visible inspection of radar images by experts often lead to misclassifications. Such an experience was made, e.g., during the oil pollution surveillance exercise CEPCO (Coordinated Extended Pollution Control Operation), which took place in the North Sea in August 2013 (http://www.schiffsjournal.de/internationale-oluberwachungsfluge-enden-erfolgreich). The aim of this exercise was to test the reliability of identifying mineral oil spills from airplanes. In this exercise, oil pollution surveillance planes from Germany, The Netherlands, Denmark, Sweden, Finland and Estonia equipped with real aperture radars (RARs) overflew for 74 h shipping lanes with the aim to locate illegal oil spills from ships. The crew reported 5 oil slicks, but it turned out that only in two cases the material floating on the sea surface was mineral oil, in two other cases it was palm oil, and in one case it was fish oil (probably associated with fishing operations).

Another example of high rates of misclassification can be found on the website of the European Maritime Safety Agency (EMSA), which operates CleanSeaNet, which is the most comprehensive oil spill monitoring and polluter identification service in Europe that supplies over 2000 analyzed satellite radar images a year to 28 participating states (http://www.emsa.europa.eu/csn-menu/csn-background.html). When CleanSeaNet detects a possible oil spill on a spaceborne SAR image, an alert message is delivered to the relevant country, which then often sends an oil pollution surveillance plane (and in some cases also a

helicopter or a ship) to the site for verification. In Europe, there exist a fleet of around 15 oil pollution surveillance planes, most of them are equipped with a suit of sensors including RAR, infrared (IR) and ultraviolet (UV) line scanners, microwave radiometer (MWR), forward-looking infrared (FLIR) sensor, laser fluorosensor (LFS), a low-light-level television camera (LLLTV) to operate in the UV range, and video and digital cameras. For example, in 2009, CleanSeaNet issued 2105 spill alerts and in 775 cases verifications were performed. However, only in 195 cases (26%) the spills could be verified as mineral oil spills. A similar low success rate is reported by Carpenter (2016): In the period from 2007 to 2010, the proportion of oil spills in German waters that were checked by aerial surveillance and verified as oil was only 35% of all spills detected by satellite. A somewhat better success rate was achieved by the Canadian Ice Service (Cao et al., 2016). The analysis of Radarsat images acquired between 2003 and 2004 provided the result that only 66% of the suspected oil spills were labeled accurately.

9. Discussion and summary

It is a highly demanding task to determine whether dark areas visible on SAR images result from mineral oil spills or oil spill look-alikes. Biogenic slicks are the most intricate oil spill look-alikes, since their radar signatures can be quite similar to those of mineral oil films. Using differences in the reduction of the NRCS, position/shape, and texture often yield misclassifications. In this paper, we have presented some representative SAR images showing radar signatures of mineral oil films and biogenic slicks. Throughout the paper, we have stressed that instrument noise is a serious issue that might have affected results obtained by previous authors using spaceborne fully-polarimetric SAR data, particularly those which include the use of cross-polarization data. Often radar signals backscattered from film-covered sea surfaces are so weak, in particular at cross-polarization, that they are near or below the noise level of the SAR.

All spaceborne multi-polarization SARs that have been used previously in fully-polarimetric SAR studies of oil spills have relatively high noise floors or high NESZ values compared to the airborne UAVSAR of NASA/JPL. The C-band SAR of the SIR-C/X-SAR Spaceshuttle mission had an NESZ of -28 dB, the L-band PALSAR onboard ALOS-1 an NESZ of -30 dB, the X-band SAR onboard TerraSAR-X has an NESZ of -19 dB $\pm$ 3 dB, and the C-band SAR onboard Radarsat-2 has an NESZ of -35 dB $\pm$ 3 dB (Migliaccio et al., 2015). Thus, data obtained from these SARs are prone to be affected by instrument noise when examining areas of low radar backscatter.

On the other hand, the airborne UAVSAR has an NESZ of -53 dB and therefore data retrieved from this SAR are unlikely to be affected by instrument noise. Minchew et al. (2012) has shown that many results obtained previously from the analysis of spaceborne SAR data are not confirmed by UAVSAR data. In particular, the UAVSAR data do not show deviations from Bragg scattering for scattering from mineral oil films, as also shown in more recent studies (e.g. Skrunes et al., 2016; Espeseth et al., 2017), which contradicts the previous findings of Migliaccio et al. (2009, 2015), Zhang et al. (2011), and Skrunes et al. (2014). However, the UAVSAR data were acquired at L-band and not at C-band as the SIR-C/X-SAR data analyzed by Migliaccio et al. (2009) and the Radarsat-2 data analyzed by Skrunes et al. (2014). Thus, one might argue that these data are not comparable. However, from a theoretical point of view as well as from the numerous radar backscattering measurements carried out in the past, there are no indications that radar backscattering from film-covered sea surfaces as well as from clean sea surfaces is fundamentally different at L- and C-band (Latini et al., 2016).

Already Gade et al. (1998b), who have analyzed multi-polarization L-and C-band data from the SIR-C/X-SAR mission in 1994, have shown that Bragg scattering dominates scattering from oil-free sea surfaces as well as from sea surfaces covered with monomolecular slicks and mineral oil films at L-and C-band. They calculated the image intensity as a function of the ellipticity and the orientation angles and showed that, for intermediate incidence angles and low to intermediate wind speeds, the co-polarization signatures of film-free and film-covered sea surfaces are similar at L- and C-band. (For the definition of polarimetric parameters, the reader is referred to the papers of van Zyl et al. (1987) and Zebker and van Zyl (1991).

The concept, that L-, C- and X-band radar backscattering from the sea surface at intermediate incidence angles and at low to medium wind speeds can be described by two-scale Bragg scattering theory, has largely been maintained over several decades (Plant et al., 2010; Plant and Irisov, 2017). Recent efforts led by Kudryavtsev and coworkers (Kudryavtsev et al., 2003, 2004; Mouche et al., 2006) suggest that a different radar backscattering mechanism applies at C-and X-band, which is related to wave breaking and is valid even for incidence angles below 50° and wind speeds below 7 m/s. In recent studies (Hansen et al., 2016; Ivonin et al., 2016) it was suggested that the reduction of NP scattering by surface films has the potential to be used for discriminating between different film types of surface films. Indeed, Radarsat- 2 and TerraSAR (X-band) SAR data analyzed by Skrunes et al. (2015) show that NP scattering caused by wave breaking is affected by surface films. But, so far, no results have been presented showing that discrimination between mineral oil films and biogenic slicks can be achieved by employing this new radar scattering theory.

Another factor that complicates unambiguous detection of mineral oil films is the fact that mineral oil films will experience complex physical, chemical, and biological processes and also interact with the ocean environment. Therefore, change will occur due to the chemical and physical processes as well as the physical characteristics of the mineral oil during the time that it is in the ocean environment. The characteristics of mineral oil on the ocean surface depend on many factors: 1) geophysical factors such as wind, waves, currents, SST, and their variations in space and time, over the oil-covered region; 2) satellite - instrument specific factors, such as the frequency, polarization, and incidence and azimuth angles; and 3) the crude oil type, volume, age, and thickness of the surface oil. In terms of monitoring, simulating and predicting crude oil spills on the ocean surface, the ideal observations should begin at the first appearance of the oil spills and end at the complete disappearance of the oil spills from the ocean environment, including after any clean-up procedures that may be undertaken. However, we are limited by our observations; we often observe the mineral oil films at a certain (often later) stage in its development cycle, and under certain very specific conditions. Thus, in principle, the scattering mechanism could be different for the different stages of the mineral oil films.

However, we believe that it is not convincing currently that double-bounce scattering enters into the radar scattering from sea surfaces covered with mineral oil films at intermediate incidence angles (see, e.g., Zhang et al., 2011; Li et al., 2015). We suspect that noise-contaminated data have led to this conclusion. Arguments in favor of this supposition can be found in the paper by Li et al. (2015), who analyzed Radarsat-2 data acquired over mineral oil films originating from oil seeps in the Gulf of Mexico and from the DWH accident. They concluded that scattering from oil originating from oil seeps is dominated by double-bounce scattering, while scattering from oil films originating from the DWH accident is dominated by Bragg scattering. But we suspect that the difference results from the difference in incidence angles: the oil seep data were acquired at an incidence angle around 43°, while the DWH data were acquired at an incidence angle around 30°. In the first case the data are very likely affected by instrument noise, but not in the second case. Thus, in both cases, Bragg scattering should apply, which is in accordance with results obtained from UAVSAR data acquired over mineral oil films in the Gulf of Mexico (Minchew et al., 2012).

However, differences in the statistical behavior of the PDF of the CPD between mineral oil films and monomolecular surface films, which have been reported by several investigators (Migliaccio et al., 2011;

Skrunes et al., 2014) could be real and not noise-related since they involve no cross-polarization data. In our view, the differences are not caused by differences in the scattering mechanism, but by differences in the statistics of the radar backscatter due to the inhomogeneity of the scattering medium. Therefore, the STD of the CPD has the potential to be used for discrimination purposes.

In our view, no convincing arguments have been presented so far in the literature, which show that non-Bragg scattering mechanisms enter into the radar backscattering from mineral oil films at intermediate incidence angles and at low to intermediate wind speeds. When inspecting critically the plots of entropy (H), anisotropy (A), and mean scattering angle (α) derived from spaceborne polarimetric SAR data, we cannot see that, in the case of radar scattering from mineral oil films, they show a clear trend towards non-Bragg scattering. For example, Zhang et al. (2011) measured H values between 0.80 and 0.95 and α values between 50° and 60°. When inserting these values into a plot of the H/α space, which is often used to identify scatter mechanisms (Pottier, 2007), then one can see that these values lie outside the dihedral scattering domain, which is characterized by $0.0 \leq H \leq 0.5$ and $50^\circ \leq \alpha \leq 90^\circ$.

Furthermore, also the PDF of the CPD shows no sign of dihedral scattering. For dihedral scattering the PDF of the CPD should be centered at 180°, which is not observed in radar scattering from mineral oil films (Migliaccio et al., 2009).

Another issue that has been addressed in this paper is whether discrimination is possible by using the difference in the dielectric constant of oil and water. It has been argued that this is possible only when the mineral oil film is sufficiently thick (for C-band, thicker than 1 mm) such that the radar signal is sensitive to the dielectric constant of the oil. However, most often the oil films are thinner such that the radar backscatter is not sensitive to the dielectric constant of the oil. Furthermore, when oil is entrained in water forming emulsion or mousse, then the dielectric constant of mineral oil also enters into scattering process in the form of an effective dielectric constant, which is determined by the oil/water mixing ratio. In this case discrimination is feasible by using dual-polarization data as provided, e.g., by Radarsat-2, TerraSAR-X, and SkyMed. It is unfortunate that the C-band SAR onboard the European Sentinel-1 satellites cannot operate in a mode, where HH and VV data can be acquired simultaneously. Thus, this technique cannot be applied using Sentinel-1 data. However, it will be possible by using ALOS-2 PALSAR data and, in the future, using Radarsat Constellation data.

A recent experiment conducted in the North Sea highlights the difficulty of separating emulsified oil from plant oil due in large part to the high winds encountered. Skrunes et al. (2016) utilized aircraft data of the UAVSAR in conjunction with coincident polarimetric data of Radarsat-2 and TerraSAR-X of three small releases of emulsified mineral oil with varying concentrations and one release of plant oil. The detectability was best in the two sensors with highest resolution, i.e., TerraSAR-X and UAVSAR. The high wind allowed for large signal-to-noise ratios over the slicks in all three sensors, even in the satellite data and in cross-polarization channels. Although detection was possible, discrimination between different types of surface films was not feasible under these conditions in any of the sensors. We note, however, that the shapes and drift patterns of the emulsified oil slicks were distinct from the monomolecular plant oil, due in part to wave mixing and retention differences in the upper ocean, thus providing a clear visual discrimination (Jones et al., 2016).

Finally, we want to comment on using plant oil to simulate biogenic slicks. Skrunes et al. (2015, 2016) used in their controlled oil experiments plant oil which is specified as a 2-ethyl-hexyl oleate (a monoalkyl ester of an oleic acid). This substance clearly has molecules with hydrophobic and hydrophilic characteristics and thus can form monolayers, but it is not known how suitable this substance is for simulating biogenic slicks. The value of its complex dilational modulus E, which determines the degree of damping, has not been reported. We suppose that the damping induced by this substance is lower than that by biogenic slicks since the measurements of Skrunes et al. (2014) always show less damping by plant oil films than by mineral oil films/emulsions, which is not typical for biogenic slicks. Probably the damping by this kind of plant oil is lower than by oleyl alcohol, which is the substance most often used to simulate biogenic slicks. Maximum damping for this substance has been determined to be −12.8 dB (Gade et al., 1998a). But there are indications that biogenic slicks damp the C-band Bragg waves even more strongly than oleyl alcohol films as shown by measurements carried out with an airborne scatterometer (Hühnerfuss et al., 1996) and with the SAR onboard the ERS-1 satellite (Espedal et al., 1998). Thus plant (palm) oil may not be the ideal substance to simulate biogenic slicks.

10. Conclusions

We conclude from the arguments presented in this paper that, in our view, fully-polarimetric or quad-polarimetric spaceborne SARs do not have the anticipated potential to significantly improve oil spill detection, particularly the separation of mineral oil from natural biogenic films. The same applies for compact-polarimetric or hybrid-polarity spaceborne SARs (Espeseth et al., 2017), which have the advantage of increased swath width, but the disadvantage of slightly decreased polarimetric performance (Collins et al., 2013). The strength of SAR polarimetry lies in its ability to identify and separate scattering mechanisms which determine the radar signatures of targets. This has led in the past to impressive results in classification of land targets (Evans et al., 1988; Cloude and Pottier, 1997; Haldar et al., 2014). However, in the case of radar backscattering from sea surfaces, whether covered with mineral oil films, biogenic slicks or film-free, there seems to be primarily only one kind of scattering mechanism present, which is surface scattering. In the incidence angle range from 20° and 50° and wind speeds below 7 m/s, the surface scattering is Bragg scattering, or more precisely, composite-surface or two-scale Bragg scattering. We challenge statements made by other authors that non-Bragg scattering is a significant contributor to radar backscattering from oil-covered sea surfaces at low to intermediate wind speeds. We hypothesize that these authors arrived at these results because they used noise-contaminated data. This point of view is supported by results using the low-noise UAVSAR over oil films in the Gulf of Mexico (Minchew et al., 2012). When analyzing SAR data from low-backscatter areas, the signal-to-noise ratio (S/N) is the relevant parameter for determining whether the results are affected by instrument noise. The S/N is a function of incidence angle, polarization, and wind speed. The higher the incidence angle and the lower the wind speed, the lower is the S/N. The S/N is particularly low at cross-polarization and thus polarimetric parameters into which cross-polarization NRCS values enter, are prone to be affected by instrument noise. This is less likely for polarimetric parameters into which only co-polarization NRCS values enter, like the co-polarized phase difference (CPD). Concerning scattering from breaking waves, we acknowledge that deviations from Bragg scattering occurs. But it is not clear whether the modification of non-polarized (NP) scattering by surface films can be used for discriminating between mineral oil films and biogenic slicks. This needs more investigations using low-noise SAR systems.

Although we expect no difference in the radar backscattering mechanism, we expect differences in the statistical behavior of radar backscattering from mineral oil films and biogenic surface films due the fact that mineral oil films usually have variable thickness and that radar backscattering from them is more inhomogeneous than from monomolecular biogenic surface films. In emulsions, the inhomogeneity in the radar backscatter may also be caused by variations of the effective dielectric constant due to variations in the oil/water mixing ratio. A method to measure this difference in the statistical behavior of radar backscatter is by means of the STD of the CPD. But, in general, it should be quite difficult to separate target-induced radar signal fluctuations

from the speckle-induced ones, especially when the oil film area is small. Thus, we are skeptical that the STD of the CPD can serve as a robust discriminator to separate oil films from biogenic slicks. However, this issue should be studied further by using data of low-noise airborne fully-polarimetric SARs, like the UAVSAR of NASA/JPL or the fully-polarimetric modular SAR system of the German Aerospace Center (DLR), which operates at X-, C-, S-, L- and P-bands (http://www.dlr.de/hr/en/desktopdefault.aspx/tabid-2326/3776_read-5691).

Recently, a method has been proposed to detect thick oil films and emulsions by employing dual-polarization SAR data (Minchew et al., 2012; Minchew, 2012). This method does not require cross-polarization data and thus it is less susceptible to instrument noise. Therefore it should be a viable method to detect thick oil films and emulsions, even with SARs that do not have an extremely low noise floor. There appears to be considerable value in the continued examination of dual polarization SARs, particularly using HH and VV channels, for both quantification of thicker oil films and emulsions as well as discrimination between mineral oil films and biogenic slicks.

In order to improve oil spill detection using SAR, we recommend to upgrade conventional oil spill detection algorithms using single-polarization SARs by including more ancillary information, like information on 1) the chlorophyll-a distribution (as a proxy for the likely presence of biogenic slicks), 2) the location of oil platforms, oil terminals, and oil seeps, 3) the sea surface current field, 4) the sea surface wind field, 5) the location of sandbanks (which appear dark on SAR images acquired during ebb tide), 6) the location of current fronts (which often manifest themselves as dark lines on SAR images), 7) the air-sea temperature difference (which affects the sea surface roughness; a negative value causes a reduction of the NRCS), 8) the rain distribution (by using weather radar images), and 9) information on ship traffic (as provided, e.g., by the Automatic Identification System (AIS)). Furthermore, near-daily repeat SAR observations with single (HH or VV) polarization SARs having large swath widths would greatly improve oil spill detection.

Acknowledgments

We thank ESA for providing the ERS and Envisat ASAR images free of charge within the ESA/NRSCC (China) DRAGON 3 project and NERSC in Bergen for giving us access to their Envisat ASAR archive. We also thank the four reviewers, whose critical comments were very helpful in improving the paper. This research was carried out in part at the Jet Propulsion Laboratory, California Institute of Technology, under contract with the National Aeronautics and Space Administration.

References

Alpers, W., 2014. Remote sensing of African coastal waters using active microwaves instruments. In: Barale, V., Gade, M. (Eds.), Satellite Observations of the African Seas. Springer, Heidelberg, pp. 75–94. Chapter 4. http://dx.doi.org/10.1007/978-94-017-8008-7_4.

Alpers, W., Espedal, H.A., 2004. Oils and surfactants. In: Jackson, C.R., Apel, J.R. (Eds.), Synthetic Aperture Radar Marine User's Manual. U.S. Department of Commerce, National Oceanic and Atmospheric Administration, Washington DC, USA, pp. 263–275 Chapter 11.

Alpers, W., Hühnerfuss, H., 1988. Radar signatures of oil films floating on the sea surface and the Marangoni effect. J. Geophys. Res. 93, 3642–3648.

Alpers, W., Hühnerfuss, H., 1989. The damping of ocean waves by surface films: a new look at an old problem. J. Geophys. Res. 94, 6251–6265.

Alpers, W., Brandt, P., Lazar, A., Dagorne, D., Sow, B., Faye, S., Hansen, W., Rubino, A., Poulain, P.-M., Brehmer, P., 2013. A small-scale oceanic eddy off the coast of West Africa studied by multi-sensor satellite and surface drifter data. Remote Sens. Environ. 129, 132–143. http://dx.doi.org/10.1016/j.rse.2012.10.032.

Alpers, W., Zhang, B., Mouche, A., Zeng, K., Chan, P.W., 2016. Rain footprints on C-band synthetic aperture radar images of the ocean - revisited. Remote Sens. Environ. 187, 169–185. http://dx.doi.org/10.1016/j.rse.2016.10.015.

ASCE, 1996. State-of-the-art review of modeling transport and fate of oil spills. J. Hydraul. Eng. 122, 594–609.

Brekke, C., Solberg, A., 2005. Oil spill detection by satellite remote sensing. Remote Sens. Environ. 95, 1–13.

Brekke, C., Solberg, A., 2008. Classifiers and confidence estimation for oil spill detection in Envisat ASAR images. IEEE Geosci. Remote Sens. Lett. 5, 65–69. http://dx.doi.org/10.1109/LGRS.2007.907174.

Cao, Y., Lilin, X., Clausi, D., 2016. Active learning for identifying mineral oil spills using 10-years Radarsat data. In: Paper Presented at the International Geoscience and Remote Sensing Symposium 2016 (IGARSS 2016), Beijing, China.

Carpenter, A., 2016. European maritime safety agency CleanSeaNet activities oil pollution in the North Sea. Oil pollution in the North Sea. In: Carpenter, A. (Ed.), The Handbook of Environmental Chemistry, 41. Springer International Publishing, Cham, pp. 33–48. http://dx.doi.org/10.1007/698_2.

Clemente-Colon, P., 2004. Upwelling. In: Jackson, C.R., Apel, J.R. (Eds.), Synthetic Aperture Radar Marine User's Manual. U.S. Department of Commerce, National Oceanic and Atmospheric Administration, Washington, DC, USA, pp. 221–244 Chapter 9.

Cloude, S.R., Pottier, E., 1996. A review of target decomposition theorems in radar polarimetry. IEEE Trans. Geosci. Remote Sens. 34, 498–518.

Cloude, S.R., Pottier, E., 1997. An entropy based classification scheme for land applications of polarimetric SAR. IEEE Trans. Geosci. Remote Sens. 35, 68–78.

Collins, M.J., Denbina, M., Atteia, G., 2013. On the reconstruction of quad-pol SAR data from compact polarimetry data for ocean target detection. IEEE Trans. Geosci. Remote Sens. 51, 591–600.

DiGiacomo, P.M., Holt, B., 2001. Satellite observations of small coastal ocean eddies in the Southern California Bight. J. Geophys. Res. 106, 22,521–22,544.

DiGiacomo, P.M., Washburn, L., Holt, B., Jones, B.H., 2004. Coastal pollution hazards in southern California observed by SAR imagery: stormwater plumes, wastewater plumes, and natural hydrocarbon seeps. Mar. Pollut. Bull. 49, 1013–1024.

Espedal, H.A., Wahl, T., 1999. Satellite SAR oil spill detection using wind history information. Int. J. Remote Sens. 20, 49–65.

Espedal, H.A., Johannessen, O.M., Johannessen, J.A., Dano, E., Lyzenga, D.R., Knulst, J.C., 1998. COASTWATCH'95: ERS 1/2 SAR detection of natural film on the ocean surface. J. Geophys. Res. 103, 24969–24982. http://dx.doi.org/10.1029/98JC01660.

Espeseth, M.M., Skrunes, S., Jones, C.E., Brekke, C., Holt, B., Doulgeris, A.P., 2017. Analysis of evolving oil spills in full-polarimetric and hybrid-polarity SAR. IEEE Trans. Geosci. Remote Sens. 55, 4190–4210. http://dx.doi.org/10.1109/TGRS.2017.2690001.

Evans, D.l., Farr, T.G., van Zyl, J.J., Zebker, H.A., 1988. Radar polarimetry: analysis tools and applications. IEEE Trans. Geosci. Remote Sens. 26, 774–789.

Franceschetti, G., Iodice, A., Riccio, D., Ruello, G., Siviero, R., 2002. SAR raw signal simulation of oil slicks in ocean environments. IEEE Trans. Geosci. Remote Sens. 40, 1935–1949.

Gade, M., Alpers, W., Hühnerfuss, H., Lange, P.A., 1998a. Wind wave tank measurements of wave damping and radar cross sections in the presence of monomolecular surface films. J. Geophys. Res. 103, 3167–3178. http://dx.doi.org/10.1029/97JC01578.

Gade, M., Alpers, W., Hühnerfuss, H., Masuko, H., Kobayashi, T., 1998b. Imaging of biogenic and anthropogenic ocean surface films by the multi-frequency/multi-polarization SIR-C/X-SAR. J. Geophys. Res. 103 (18) (851-18 866).

Garcia-Pineda, O., MacDonald, I., Hu, C., Svejkovsky, J., Hess, M., Dukhovskoy, D., Morey, S.L., 2013. Detection of floating oil anomalies from the Deepwater Horizon oil spill with synthetic aperture radar. Oceanography 26 (2). http://dx.doi.org/10.5670/oceanog.2013.

Gierach, M., Holt, B., Trinh, R., Pan, B.J., Rains, C., 2017. Satellite detection of wastewater diversion plumes in Southern California. Estuar. Coast. Shelf Sci. 186, 171–182. http://dx.doi.org/10.1016/j.ecss.2016.10.012.

Haldar, D., Das, A., Yadav, M., Hooda, S.H., Mohan, S., Chakraborty, M., 2014. Analysis of temporal polarization phase difference for major crops in India. Prog. Electromagn. Res. B 57, 299–309.

Hansen, M.W., Kudryavtsev, V., Chapron, B., Brekke, C., Johannessen, J.A., 2016. Wave breaking in slicks: impacts on C-band quad-polarized SAR measurements. IEEE J. Sel. Top. Appl. Earth Obs. Remote Sens. 9, 4029–4040. http://dx.doi.org/10.1109/JSTARS.2016.2587840.

Holt, B., Trinh, R., Gierach, M., 2017. Satellite analysis of stormwater runoff plumes in Southern California detected with SAR and MODIS imagery. Mar. Pollut. Bull. 118, 141–154. http://dx.doi.org/10.1016/j.marpolbul.2017.02.040.

Hühnerfuss, H., Alpers, W., Dannhauer, H., Gade, M., Lange, Ph.A., Neumann, V., Wismann, V., 1996. Natural and man-made sea slicks in the North Sea investigated by a helicopter-borne 5-frequency radar scatterometer. Int. J. Remote Sens. 17, 1567–1582. http://dx.doi.org/10.1080/01431169608945364.

ITOPF, 2014. Technical information paper (TIPS). In: Fate of Oil Spills, . http://www.itopf.com/fileadmin/data/Documents/TIPS%20TAPS/TIP2FateofMarineOilSpills.pdf.

Ivonin, D.V., Skrunes, S., Brekke, C., Ivanov, A.Yu., 2016. Interpreting sea surface slicks on the basis of the normalized radar cross-section model using Radarsat-2 co-polarization dual-channel SAR images. Geophys. Res. Lett. 43, 2748–2757. http://dx.doi.org/10.1002/2016GL068282.

Jakeman, E., Pusey, P.N., 1976. A model for non-Rayleigh sea echo. IEEE Trans. Antennas Propag. 4, 806–814.

Jenkins, A.D., Dyste, K.B., 1997. The effective film viscosity coefficients of a thin floating fluid layer. J. Fluid Mech. 344, 335–337.

Jenkins, A.D., Jacobs, A.S., 1997. Wave damping by a thin layer of viscous fluid. Phys. Fluids 9, 1256–1264.

Jones, C.E., Dagestad, K.-F., Breivik, Ø., Holt, B., Roehrs, J., Christensen, K.H., Espeseth, M., Brekke, C., Skrunes, S., 2016. Measurement and modeling of oil slick transport. J. Geophys. Res. Oceans 121, 7759–7775. http://dx.doi.org/10.1002/2016JC012113.

Karimova, S., 2012. Spiral eddies in the Baltic, Black and Caspian seas as seen by satellite radar data. Adv. Space Res. 50, 1107–1124.

Kim, T., Park, K., Li, X., Lee, M., Hong, S., Lyu, S., Nam, S., 2015. Detection of the Hebei Spirit oil spill on SAR imagery and its temporal evolution in a coastal region of the Yellow Sea. Adv. Space Res. 56, 1079–1093. http://dx.doi.org/10.1016/j.asr.2015.

05.040.
Kudryavtsev, V., Johannessen, J.A., 2004. On effect of wave breaking on short wind waves. Geophys. Res. Lett. http://dx.doi.org/10.1029/2004GL020619.
Kudryavtsev, V., Hauser, D., Caudal, G., Chapron, B., 2003. A semi-empirical model of the normalized radar cross-section of the sea surface, 1. Background model. J. Geophys. Res. 108, 8054. http://dx.doi.org/10.1029/200IJCOOI003.
Kurata, N., Vella, K., Shivji, M., Soloviev, A., Matt, S., Tartar, A., Perrie, W., 2016. Surfactant-associated bacteria in the near-surface layer of the ocean. Sci Rep 6, 19123. http://dx.doi.org/10.1038/srep19123.
Latini, D., Del Frate, E., Jones, C.F., 2016. Multi-frequency and polarimetric quantitative analysis of the Gulf of Mexico oil spill event comparing different SAR systems. Remote Sens. Environ. http://dx.doi.org/10.1016/j.rse.2016.05.014.
Lee, J.-S., Pottier, E., 2009. Polarimetric Radar Imaging, From Basics to Applications. CRC Press, Boca Raton, FL, USA.
Leifer, I., Lehr, B., Simecek-Beatty, D., Bradley, E., Clark, R., Dennison, P., Hu, Y., Matheson, S., Jones, C., Holt, B., Reif, M., Roberts, D., Svejkovsky, J., Swayze, G., Wozencraft, J., 2012. State of the art satellite and airborne marine oil spill remote sensing: application to the BP Deepwater Horizon oil spill. Remote Sens. Environ. 124, 185–209. http://dx.doi.org/10.1016/j.rse.2012.03.024.
Li, H., Perrie, W., He, Y., Wu, J., Luo, X., 2015. Analysis of the polarimetric SAR scattering properties of oil-covered waters. IEEE J. Sel. Top. Appl. Earth Obs. Remote Sens. 8, 3751-375. http://dx.doi.org/10.1109/JSTARS.2014.2348173.
Lin, I.-I., Wen, L.S., Liu, K.-K., Tsai, W.-T., Liu, A., 2002. Evidence and quantification of the correlation between radar backscatter and ocean colour supported by simultaneously acquired in situ sea truth. Geophys. Res. Lett. 29. http://dx.doi.org/10.1029/2001GL014039.
Lin, I.-I., Alpers, W., Liu, T.W., 2003. First evidence for the detection of natural surface films by the QuikSCAT scatterometer. Geophys. Res. Lett. 30, 1713 (doi: 1029/2003GL017415).
MacDonald, I.R., et al., 2015. Natural and unnatural oil slicks in the Gulf of Mexico. J. Geophys. Res. Oceans 120, 8364–8380. http://dx.doi.org/10.1002/2015JC011062.
Migliaccio, M., Ferrara, G., Gambardella, A., Nunziata, F., Sorrentino, A., 2007. A physically consistent speckle model for marine SLCS SAR images. IEEE J. Ocean. Eng. 32, 839–847.
Migliaccio, M., Nunziata, F., Gambardella, A., 2009. On the co-polarized phase difference for oil spill observation. Int. J. Remote Sens. 30, 1587–1602.
Migliaccio, M., Nunziata, F., Montuori, A., Li, X., Pichel, W.G., 2011. Multi-frequency polarimetric SAR processing chain to observe oil fields in the Gulf of Mexico. IEEE Trans. Geosci. Remote Sens. 49, 4729–4737.
Migliaccio, M., Nunziata, F., Buono, A., 2015. SAR polarimetry for sea oil slick observation. Int. J. Remote Sens. 36, 3243–3273. http://dx.doi.org/10.1080/01431161.2015.105730.
Minchew, B., 2012. Determining the mixing of oil and sea water using polarimetric synthetic aperture radar. Geophys. Res. Lett. 39, L16607. http://dx.doi.org/10.1029/2012GL052304.
Minchew, B., Jones, C.E., Holt, B., 2012. Polarimetric analysis of backscatter from the Deepwater Horizon oil spill using L-band synthetic aperture radar. IEEE Trans. Geosci. Remote Sens. 50, 3812–3830.
Mouche, A.A., Hauser, D., Kudryavtsev, V., 2006. Radar scattering of the ocean surface and sea-roughness properties: a combined analysis from dual-polarizations airborne radar observations and models in C band. J. Geophys. Res. Oceans 111, C09004.
Munk, W., 2001. Spirals on the sea. Sci. Mar. 65, 193–198.
Munk, W., Armi, L., Fischer, K., Zachariasen, F., 2000. Spirals on the sea. Proc. R. Soc. London A Math. Phys. Eng. Sci. 446, 1217-180.
NOAA Hazmat, 2012. Open Water Oil Identification Job Aid for Aerial Observation. Office of Response and Restoration. Available at. http://response.restoration.noaa.gov/sites/default/files/OWJA_2012.pdf, Version 2.
Nunziata, F., Gambardella, A., Migliaccio, M., 2008. On the Mueller scattering matrix for SAR sea oil slick observation. IEEE Geosci. Remote Sens. Lett. 5, 691–695.
Oliver, J.K., Willis, B.L., 1987. Coral-spawn slicks in the great barrier reef: preliminary observations. Mar. Biol. 94, 521–529.
Plant, W.J., Irisov, V., 2017. A joint active/passive physical model of sea surface microwave signatures. J. Geophys. Res. Oceans. http://dx.doi.org/10.1002/2017JC012749.
Plant, W.J., Keller, W.C., Hayes, K., Chatham, G., 2010. Normalized radar cross section of the sea for backscatter: 1. Mean levels. J. Geophys. Res. Oceans 115, C09032. http://dx.doi.org/10.1029/2009JC006078.
Pottier, E., 2007. Advanced Training Course on Land Remote Sensing. Available on line. http://earth.esa.int/landtraining07/D1LA3-Pottier.pdf.
Raney, R.K., 2007. Hybrid-polarity SAR architecture. IEEE Trans. Geosci. Remote Sens. 45, 3397–3404. http://dx.doi.org/10.1109/TGRS.2007.895883.
Raney, R.K., 2016. Comparing compact and quadrature polarimetric SAR performance. IEEE Geosci. Remote Sens. Lett. 13, 861–864. http://dx.doi.org/10.1109/LGRS.2016.2550863.
Rice, S.O., 1951. Reflection of electromagnetic waves from slightly rough surfaces. Commun. Pure Appl. Math. 4, 351–378.
Romano, J.C., 1996. Sea-surface slick occurrence in the open sea (Mediterranean, Red Sea, Indian Ocean) in relation to wind speed. Deep-Sea Res. I Oceanogr. Res. Pap. 43, 411–423.
Skrunes, S., Brekke, C., Eltoft, T., 2014. Characterization of marine surface slicks by Radarsat-2 multipolarization features. IEEE Trans. Geosci. Remote Sens. 52, 5302–5319.
Skrunes, S., Brekke, C., Eltoft, T., Kudryavtsev, V., 2015. Comparing near-coincident C- and X-band SAR acquisitions of marine oil spills. IEEE Trans. Geosci. Remote Sens. 53, 1958–1974.
Skrunes, S., Brekke, C., Jones, C.E., Holt, B., 2016. A multisensor comparison of experimental oil spills in polarimetric SAR. IEEE J. Sel. Top. Appl. Earth Obs. Remote Sens. http://dx.doi.org/10.1109/JSTARS.2016.2565063.
Suresh, G., Melsheimer, C., Körber, J.-H., Bohrmann, G., 2015. Automatic estimation of oil seep locations in synthetic aperture radar images. IEEE Trans. Geosci. Remote Sens. 53, 4218–4230. http://dx.doi.org/10.1109/TGRS.2015.2393375.
Tang, D., Kester, D.R., Ni, L.-H., Kawamura, H., Hong, H., 2002. Upwelling in the Taiwan Strait during the summer monsoon detected by satellite and shipboard measurements. Remote Sens. Environ. 83, 457–471. http://dx.doi.org/10.1016/S0034-4257(02)00062-7.
Ulaby, F.T., Dobson, M.C., 1987. Handbook of Radar Scattering Statistics for Terrain. Artech House, Norwood, MA., USA.
Ulaby, F.T., Held, D., Dobson, M.C., McDonald, K.C., and. Thomas, B. A., 1987. Relating polarization phase difference (PPD) of SAR signals to scene properties. IEEE Trans. Geosci. Remote Sens. 25, 83–91.
Ulaby, F.T., Sarabandi, K., Nashashibi, A., 1992. Statistical properties of the Mueller matrix of distributed targets. IEEE Proc. F, Radar Signal Process. 139, 136–146.
Valenzuela, G.R., 1978. Theories for the interaction of electromagnetic and oceanic waves - a review. Bound.-Layer Meteorol. 13, 61–85.
van Zyl, J.J., Zebker, H.A., Elachi, C., 1987. Imaging radar polarization signatures: theory and observations. Radio Sci. 22, 529–543.
Velotto, D., Migliaccio, M., Nunziata, F., Lehner, S., 2011. Dual-polarized TerraSAR-X data for oil-spill observation. IEEE Trans. Geosci. Remote Sens. 49, 4751–4762.
Wang, G., Li, J., Zhang, B., Cai, Z., Zhang, F., Shen, Q., 2017. Synthetic aperture radar detection and characteristic analysis of cyanobacterial scum in Lake Taihu. J. Appl. Remote. Sens. 11 (1), 012006. 2017. http://dx.doi.org/10.1117/1.JRS.11.012006.
Wurl, O., Wurl, E., Miller, L., Johnson, K., Vagle, S., 2011. Formation and global distribution of sea-surface microlayers. Biogeosciences 8, 121–135.
Wurl, O., Stolle, Ch., Thuoc, Ch.V., Thu, Ph., Mari, X., 2016. Biofilm-like properties of the sea surface and predicted effects on air–sea CO_2 exchange. Prog. Oceanogr. 144, 15–24.
Zebker, H.A., van Zyl, J.J., 1991. Imaging radar polarimetry: a review. Proc. IEEE 79, 1583–1606.
Zhang, B., Perrie, W., Li, X., Pichel, W.G., 2011. Mapping sea surface oil slicks using Radarsat -2 quad-polarization SAR image. Geophys. Res. Lett. 38 (L10602-1–L10602-5).
Zutic, V., Cosovic, B., Marcenko, E., Bihari, N., 1981. Surfactant production by marine phytoplankton. Mar. Chem. 10, 505–520.